IMA Journal of Applied Mathematics (2011) 1–31
doi: 10.1093/imamat/hxh000

Characterising the multiscale structure of fluctuations of transported quantities in a disordered medium

IGOR L. CHERNYAVSKY[1,*], IAN L. DRYDEN[2] AND OLIVER E. JENSEN[1]

[1] *School of Mathematical Sciences, University of Nottingham, University Park, Nottingham NG7 2RD, UK*

[2] *Department of Statistics, LeConte College, University of South Carolina, Columbia SC 29208, USA*

[*] *Corresponding author: Igor.Chernyavsky@nottingham.ac.uk*

The transport of a scalar quantity in a disordered medium is a common problem in science and engineering. To understand the interplay between deterministic transport dynamics and stochasticity of the underlying microstructure, we analyse a simple model for unidirectional advection-diffusion-reaction over a random array of point sinks. The homogenized concentration distribution over a periodic array provides a leading-order approximation for a wide range of ergodic stationary random sink distributions of comparable mean density. However the fluctuations about this state depend strongly on the statistical properties of the array and the relative sizes of the scale-separation parameter (the ratio of mean inter-sink distance to domain size) and the physical parameters (expressed as dimensionless Péclet and Damköhler numbers). Using a combination of Monte Carlo simulation and asymptotic analysis, we characterise the spatial variability and correlation statistics of the transported quantity and show how the underlying regularity of the microstructure, particularly at low Péclet numbers, ensures a much smaller fluctuation magnitude than in the case of a uniformly random microstructure. Even when sink locations are almost uncorrelated to each other, we find that the concentration fluctuations correlate strongly over lengthscales comparable to the whole domain. Thus boundary conditions can determine the distributions of both the averaged leading-order distribution of the transported quantity and its fluctuations.

Keywords: advection-diffusion-reaction; stochastic homogenization; random medium; parameter regime

1. Introduction

The theory of homogenization is a combination of multiple-scales analysis and averaging techniques that has been successfully applied to a variety of physical, engineering and biomedical problems since its development in the 1970's by Babuška (1976), Bakhvalov (1974), Berdichevskii (1975), Keller (1977), Papanicolaou (1975), Sánchez-Palencia (1980) and others. Applications of homogenization are as diverse as standard equations of mathematical physics with rapidly oscillating coefficients (on a domain with periodic microstructure) (Bakhvalov & Panasenko, 1989), wave-propagation in fibre-reinforced poroelastic media (Parnell & Abrahams, 2008) and the molecular strain energy of DNA (Maddocks, 2004).

The homogenization method provides a convenient analytical tool for obtaining the effective macroscopic description of underlying phenomena at fine scales if a representative periodic structural unit at these scales can be devised, or if the assumptions of statistical homogeneity and ergodicity can be applied

21 November 2011

to the system (Torquato, 2006). The original motivation, and most common application, of the homogenization method is to the physics of composite materials (Sánchez-Palencia, 1980); here, much effort has been put into problems of convergence of differential operators and functionals in the theory of ordinary and partial differential equations with rapidly oscillating coefficients (Bakhvalov & Panasenko, 1989; Bensoussan *et al.*, 1978; Zhikov *et al.*, 1979). However, recent interest in biomechanical applications has unveiled new opportunities for averaging and homogenization approaches (Chapman *et al.*, 2008; Chernyavsky *et al.*, 2011; Shipley & Chapman, 2010; Wood *et al.*, 2002).

Homogenization techniques for media with periodic microstructure were pioneered by Maxwell (1873) and Rayleigh (1892). Since then, the effective properties of a medium with respect to heat or mass transport have been derived for a variety of transport regimes and medium compositions (Batchelor & O'Brien, 1977; Keller, 1963; Sangani & Acrivos, 1983). These are typically parametrised by a Péclet number Pe (representing the relative strength of advection to diffusion), a Damköhler number Da (representing the relative rate of a reaction to diffusion) and a scale-separation parameter $\varepsilon \ll 1$ (the ratio of microscopic to macroscopic lengthscales). Sangani, Acrivos and co-authors studied by a hybrid numerical-analytical approach the effect of flow at low Pe (Acrivos *et al.*, 1980; Sangani & Acrivos, 1982) and high Pe (Wang & Sangani, 1997) on heat transport at fixed heat-exchange rate or fixed temperature of heated spheres and cylinders arranged in periodic or random arrays. Auriault & Adler (1995) classified parameter regimes for two-dimensional advective-diffusive transport without reaction ($\mathrm{Da} = 0$). Mauri (1991) considered several different scalings of Pe and Da for first-order irreversible reaction kinetics in a periodic porous medium and obtained the corresponding effective equations. More recently, Mikelić *et al.* (2006) and Allaire & Raphael (2007) provided rigorous estimates for convergence of the homogenised solutions to an advection-diffusion-reaction problem at large macroscopic Pe and Da. Figure 1(a) illustrates how these authors have contributed descriptions of different asymptotic transport regimes across $(\mathrm{Pe}, \mathrm{Da})$ parameter space, in the context of one-dimensional transport via advection and diffusion past a periodic array of sinks with zeroth-order kinetics. This Figure also illustrates typical distinct asymptotic regimes in parameter space within which different physical effects dominate (derived in Chernyavsky *et al.*, 2011, hereafter referred to as CLDJ).

The stochastic homogenization method of Bensoussan *et al.* (1978) was proposed almost simultaneously with the development of the theory of homogenization for periodic structures. In the case of statistically homogeneous and ergodic microstructure, virtually all results for periodic porous media are directly applicable and *vice versa* (Torquato, 2006). The effective advective-diffusive transport in random flow fields was shown to have many similarities with transport in a periodic velocity field (McCarty & Horsthemke, 1988; McLaughlin *et al.*, 1985). In parallel with the homogenization technique, several statistical (Hashin & Shtrikman, 1962; Prager, 1963) and analytical (Bergman, 1980; Milton, 1981) methods for identifying rigorous bounds of effective material properties have been developed. In particular, the n-point correlation (probability) function formalism of Torquato and co-authors has assisted calculation of geometry-specific bounds (Torquato, 1991). Using the framework of generalised Taylor dispersion, Shapiro & Brenner (1988) calculated effective parameters of an advection-diffusion-reaction equation for first-order kinetics by studying the properties of statistical averages (moments) of a solute "Brownian particle" introduced into a spatially periodic porous medium. The volume averaging method by Whitaker and others (Whitaker, 1967; Zolotarev & Radushkevich, 1968) was recently applied to find effective nonlinear Michaelis–Menten-type reaction-diffusion equations in biofilms (Wood *et al.*, 2002). Meanwhile recent advances in stochastic geometry and meso-scale homogenization have allowed the development of time-dependent growth models (for applications such as a growing network of blood vessels), where global scalar fields of the medium affect the geometry of the microstructure and vice versa, providing a feedback loop across different lengthscales (Capasso, 2009); for more detailed recent reviews of homogenization and other effective description

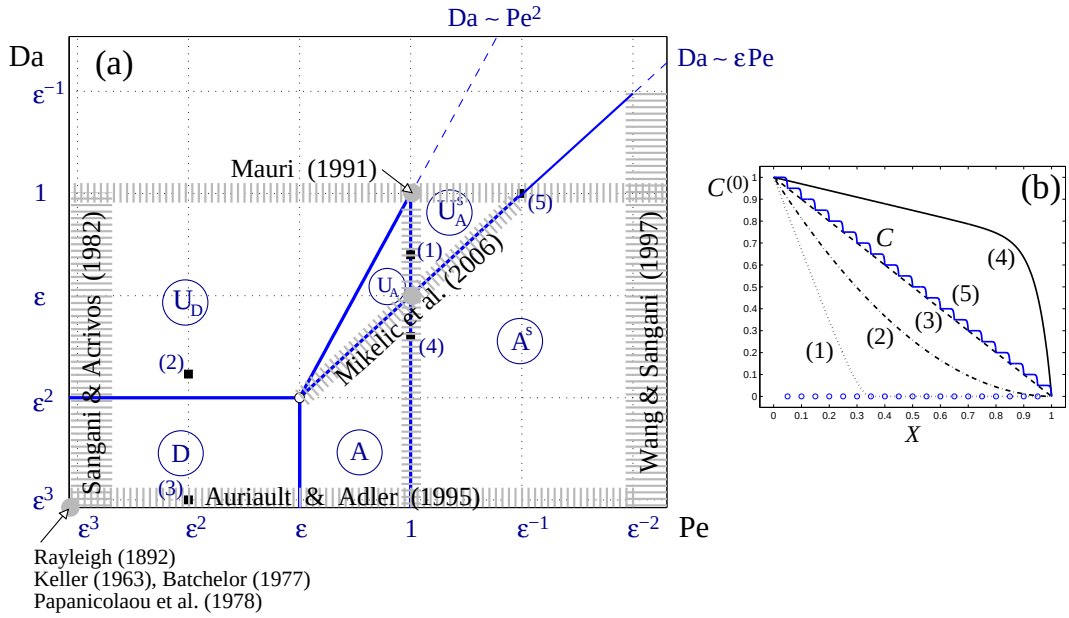

Figure 1. (a) A schematic representation of $(\mathrm{Pe}, \mathrm{Da})$-parameter ranges considered in previous studies of homogenized advection-diffusion-reaction problems. Parameter ranges addressed by previous authors (shaded grey regions and grey circles) have been "projected" on the $(\mathrm{Pe}, \mathrm{Da})$-parameter space derived in CLDJ for one-dimensional transport past a periodic array of sinks with constant uptake. (Damköhler and Péclet numbers are defined on the local inter-sink distance.) Solid lines demarcate six distinct asymptotic regimes: uptake-dominated ($\mathrm{U_D}$, $\mathrm{U_A}$, $\mathrm{U_A^s}$), diffusion-dominated (D) and advection-dominated (A, $\mathrm{A^s}$). Peripheral shaded areas represent the limits $\mathrm{Pe} \to 0$ (left), $\mathrm{Pe} \to \infty$ (right), and $\mathrm{Da} \to 0$ (bottom). (b) Leading-order homogenized solutions $C^{(0)}$ for representative points (1)-(4) in the parameter space ($\mathrm{Pe} = 1, \varepsilon^2, \varepsilon^2, 1$ and $\mathrm{Da} = \varepsilon^{0.6}, 2\varepsilon^2, \varepsilon^3, \varepsilon^{1.4}$ respectively) and the exact solution C for the point (5) ($\mathrm{Pe} = \varepsilon^{-1}$, $\mathrm{Da} = 1$), illustrating a "staircase" structure, are plotted across the spatial domain $0 < X < 1$, computed with $\varepsilon = 0.05$; circles show the locations of the 19 sinks (CLDJ).

techniques, see Chernyavsky (2011), Parnell & Abrahams (2012).

Key features of the transported scalar field over a periodic distribution of sinks are summarised in Figure 1 (adapted from CLDJ). Diffusive, advective and uptake fluxes across the whole domain balance when $\mathrm{Da} = O(\varepsilon^2)$, $\mathrm{Pe} = O(\varepsilon)$, defining an organising centre in $(\mathrm{Pe}, \mathrm{Da})$-parameter space (see Fig. 1a). A second organising centre at $\mathrm{Pe} = O(1)$, $\mathrm{Da} = O(\varepsilon)$ characterises the balance of advection and diffusion at the inter-sink scale, while advective and uptake fluxes remain balanced at the scale of entire domain. Radiating from the organising centres are the lines that bound asymptotic domains; within each domain a single physical effect typically dominates at the macroscopic lengthscale, although additional effects become important within internal boundary layers at smaller scales (as illustrated in Fig. 1b). Asymptotic analysis for other types of reaction kinetics (see Appendix A) indicates that the layout of the asymptotic domains in (Pe, Da)-space (Fig. 1a) remains broadly similar, although the specific functional form of the solution profile differs (*cf.* Figs 1(b) and A.1). As indicated above, the map of asymptotic domains applies also when sinks are distributed randomly (CLDJ). However the parameter ranges within which the homogenization approximation

is valid are sensitive to sink distributions, as we discuss further below.

In transport problems involving stochastic geometries, when the problem is posed in terms of statistical distributions, the classical homogenized solution provides information regarding the mean properties of a transported field but not the statistical properties of the fluctuations about the mean that will arise in a particular realisation of the problem. The fluctuations are important in understanding the accuracy of the homogenized solution across parameter space as well as being of practical significance in certain applications. Here, we estimate the properties of fluctuations in the context of the simple problem illustrated in Figure 1(b), which was motivated by maternal blood flow in the human placenta (CLDJ), involving transport via advection and diffusion past a distribution of sinks, when the sink locations have prescribed statistical properties (§ 2). In the first instance, numerical Monte-Carlo simulation enables us to compute the properties of fluctuations directly; the fluctuations show striking multiscale behaviour, such that the covariance varies smoothly over macroscopic lengthscales under the influence of boundary conditions. We analyse this behaviour (§ 3) by exploiting the linearity of the governing PDE, which enables the solute concentration field to be expressed as a functional of the sink locations (although this functional is, for most parameter regimes, nonlinear). Then, for a given statistical sink distribution, we approximate the statistical properties of the fluctuations by exploiting the multiscale nature of the problem. Our non-standard approach was introduced in CLDJ for the case of linear functionals; here we extend it into the nonlinear regime in some special cases, enabling us to provide convergence estimates across parameter space (§ 4).

2. Problem statement

Consider a one-dimensional array of N identical point sinks of constant strength q_0. The size of the domain is L, and l is the distance between two adjacent sinks ($l \ll L,\ L = (N+1)l$). Solute is carried past the sinks by a unidirectional flow field u_0, assumed to be uniform over the domain (as if driven by a constant pressure drop according to Darcy's law); the solute concentration C_0 at the inlet ($x^* = 0$) is prescribed, and the concentration at the outlet ($x^* = L$) is set to be zero. The solute diffuses between the sinks with diffusivity D. The concentration field $C^*(x^*)$ is required to be non-negative, and therefore, for sufficiently strong uptake, we define an internal free boundary at $x^* = x_0^*$ such that $C^* > 0$ for $0 < x^* < x_0^*$, and $C^* = 0$ for $x_0^* < x^* < L$.

Introducing non-dimensional variables $C^* = C_0 C,\ x^* = l x,\ x_0^* = l x_0$, we write the advection-diffusion-uptake problem for the solute in dimensionless form (as in CLDJ) as

$$\begin{aligned} &\frac{\mathrm{d}^2 C}{\mathrm{d}x^2} - \mathrm{Pe}\,\frac{\mathrm{d}C}{\mathrm{d}x} = \mathrm{Da}\, f(x), \quad f = \sum_{i=1}^{N} \delta(x-\xi_i), \quad 0 < x < \varepsilon^{-1}, \\ &C|_{x=0} = 1, \quad C|_{x=\varepsilon^{-1}} = 0 \ \text{ or } \ C|_{x=x_0} = \left.\frac{\mathrm{d}C}{\mathrm{d}x}\right|_{x=x_0} = 0, \end{aligned} \tag{2.1}$$

where ξ_i denotes the position of the i^{th} sink ($i = 1,\dots,N$), as illustrated in Figure 2, $\varepsilon = l/L$ and $\mathrm{Pe} = u_0 l/D$ and $\mathrm{Da} = q_0 l/(DC_0)$ are the microscopic Péclet and Damköhler numbers respectively.

A global balance of diffusive, advective and uptake fluxes (in dimensional variables) $DC_0/L \sim u_0 C_0 \sim \varepsilon^{-1} q_0$, identifies the organising centre $1 \sim \varepsilon^{-1}\mathrm{Pe} \sim \varepsilon^{-2}\mathrm{Da}$ in (Pe, Da)-parameter space (CLDJ). We look for an approximate solution to (2.1) about this point (with $\mathrm{Pe} = \varepsilon p,\ \mathrm{Da} = \varepsilon^2 q$ and $p, q = O(1)$) in the form of a two-scale asymptotic power series

$$C \equiv C^{\varepsilon}(X) = C^{(0)}(x,X) + \varepsilon C^{(1)}(x,X) + \varepsilon^2 C^{(2)}(x,X) + \dots, \quad X = \varepsilon x. \tag{2.2}$$

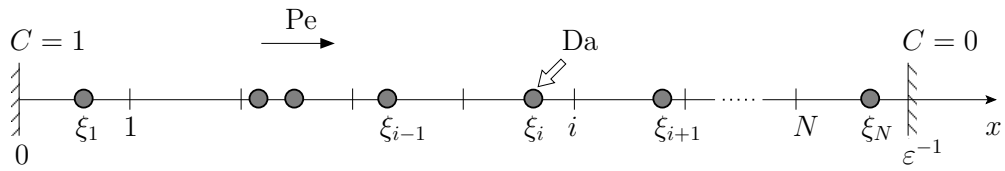

Figure 2. A schematic random array of N sinks (circles), located at $x = \xi_i$; ticks indicate the position of sinks in a periodic array of the same size (all variables are given in a dimensionless form).

Treating short and long-range spatial variables x and X as independent, the differential operators change accordingly:

$$\frac{\mathrm{d}}{\mathrm{d}x} = \frac{\partial}{\partial x} + \varepsilon \frac{\partial}{\partial X}, \quad \frac{\mathrm{d}^2}{\mathrm{d}x^2} = \frac{\partial^2}{\partial x^2} + 2\varepsilon \frac{\partial^2}{\partial x \partial X} + \varepsilon^2 \frac{\partial^2}{\partial X^2}. \tag{2.3}$$

Substituting (2.2) and (2.3) into (2.1), collecting terms in powers of ε, assuming x-periodicity (i.e. $\xi_i = i$ in (2.1)) and averaging over a unit cell, we get the leading-order solution to (2.1), given by CLDJ as

$$C^{(0)}(X) = \begin{cases} \left(\frac{q}{p} - 1\right) \dfrac{\mathrm{e}^{pX} - 1}{\mathrm{e}^{p} - 1} - \frac{q}{p} X + 1, & 0 \leqslant X \leqslant 1, \qquad \text{for} \quad q \leqslant Q(p) \\ \dfrac{q}{p^2} \dfrac{\mathrm{e}^{pX} - 1}{\mathrm{e}^{pX_0}} - \frac{q}{p} X + 1, & 0 \leqslant X \leqslant X_0, \\ 0, & X_0 < X \leqslant 1, \end{cases} \qquad \text{for} \quad q > Q(p) \tag{2.4a}$$

where

$$Q(p) = \frac{p^2 \mathrm{e}^{p}}{(p-1)\mathrm{e}^{p} + 1}, \quad X_0 = -\frac{1}{p} \mathrm{e}^{-pX_0} + \frac{q + p^2}{pq}, \quad (0 < X_0 \leqslant 1). \tag{2.4b}$$

Note that for $q = p$ (Da $= \varepsilon$Pe), expression (2.4) simplifies to the linear function $C^{(0)} \equiv 1 - X$, greatly facilitating calculations. Since an ergodic and spatially uniform (stationary) random medium has the same leading-order behaviour as the equivalent periodic medium of the same average density (Torquato, 2006), we can use (2.4) to provide a leading-order estimate of the concentration field when the sinks are distributed either periodically or randomly (in the limit $\varepsilon \to 0$). Following Pavliotis & Stuart (2008), we can then compute the fluctuations about the mean in the form of the *homogenization residue*, defined as

$$r^{\varepsilon}(X) = C - C^{(0)}. \tag{2.5}$$

We consider different types of irregular arrays in order to understand the accuracy of the homogenization description in these cases. Since we deal with point objects, it is convenient to employ standard random point processes to construct sink distributions. A natural choice is to use a *uniformly random* distribution of N sinks in the open interval $X \in (0,1)$ (see representative realisations of the solution C in Fig. 3(a) for $N = 49$ and the homogenization residue r^{ε} in Fig. 3(c) for $N = 1019$ at large Péclet number; Fig. 4(a,b) shows analogous quantities at small Pe). Another natural random distribution to consider is the normal perturbation of a periodic array (also called *normal perturbations*), where each sink is displaced normally (with a given standard deviation σ on the X-scale) about its position in a periodic array (representative

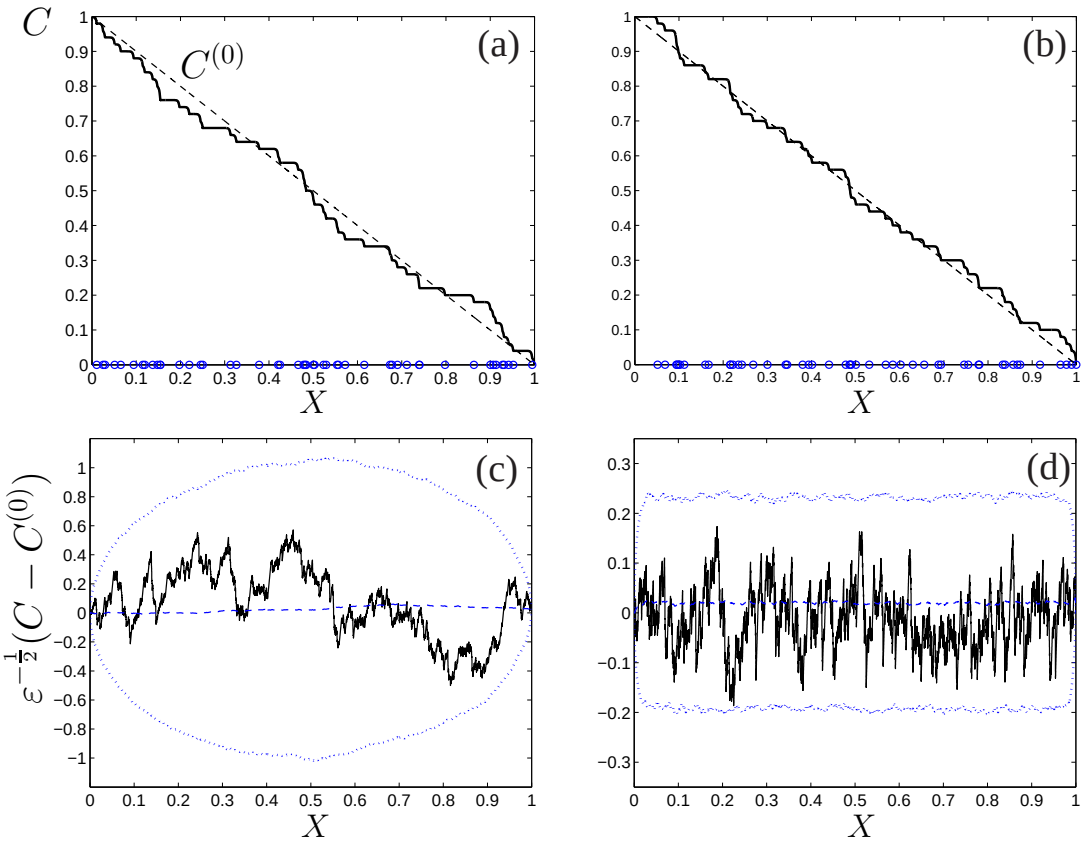

Figure 3. Simulation (solid) compared to $C^{(0)}$ (dashed) for (a) uniformly random and (b) normally-perturbed periodic ($\sigma = 10\varepsilon$) sink distributions, for $N = 49$ sinks ($\varepsilon = 0.02$), Pe $= 10$ and Da $= \varepsilon$Pe. Sinks for these realisations are shown with circles. (c,d) A single realisation of the homogenization residue $r^\varepsilon = C - C^{(0)}$ (solid) scaled by $\varepsilon^{-1/2}$, corresponding to (a,b) for $\varepsilon = 0.001$ (other parameters as in (a,b)). The dashed line shows the pointwise ensemble mean $\mathbb{E}[r^\varepsilon]$ and dotted lines show mean $\pm$ two standard deviations $\mathbb{V}\mathrm{ar}[r^\varepsilon]^{1/2}$, both computed from $N_{\mathrm{ens}} = 1000$ Monte-Carlo samples.

realisations are shown in Fig. 3(b,d) for large and in Fig. 4(b,d) for small Pe). According to the properties of a normal distribution, we expect 99% of sinks to remain in their original unit cells for $0 \leqslant \sigma \leqslant \varepsilon/6$. As σ increases, the sinks start swapping their unit cells and sorting of their new positions has to be applied. In the limit of small standard deviations ($\sigma \to 0$), the normally-perturbed array tends to an unperturbed periodic array, and a normally-perturbed array approaches a uniformly random distribution as σ/ε becomes $\gg 1$ (with periodic boundary conditions imposed upon sinks falling outside the domain). Therefore, we consider two stochastic forms of the source term f in (2.1):

(i) $f = f_u$: a uniformly-random distribution, where ξ_i are independent ordered values drawn from $\mathscr{U}[0, \varepsilon^{-1}]$;

(ii) $f = f_n(\sigma)$: a normally-perturbed periodic distribution satisfying $\xi_i \sim \mathscr{N}(i, \sigma_0^2)$, for some

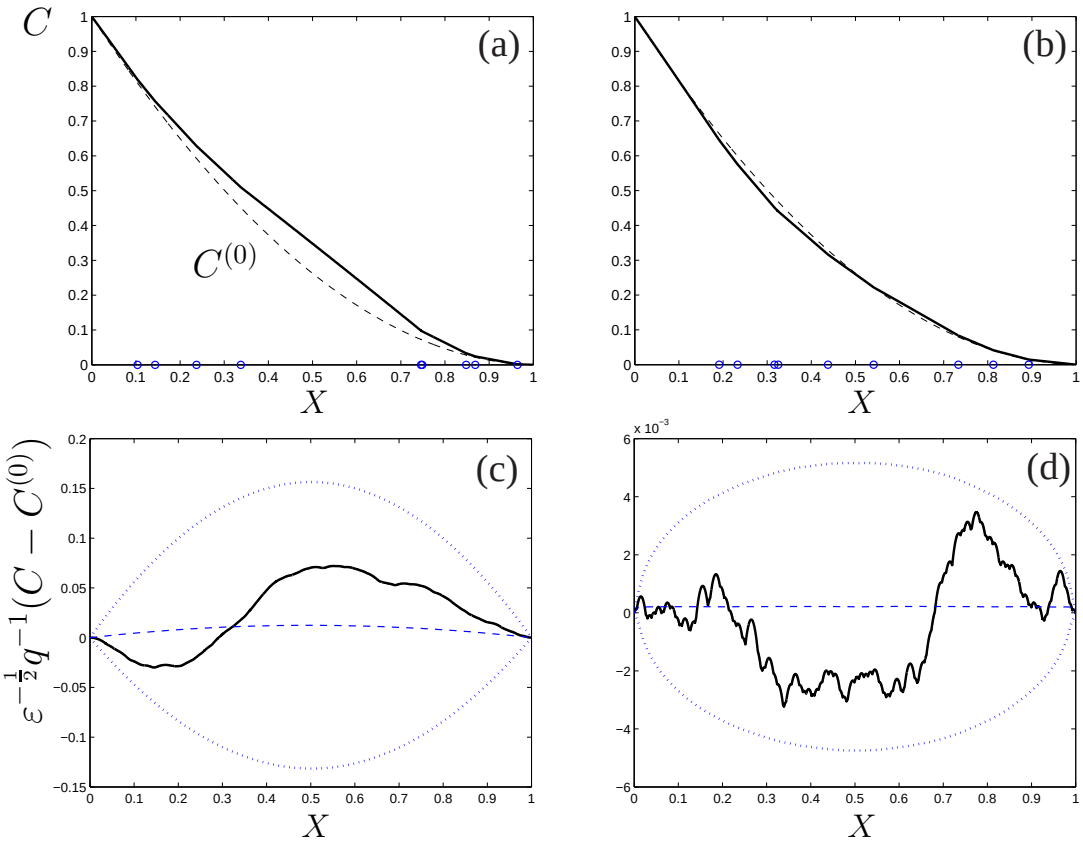

Figure 4. (a,b) Realisations of the solute profile C (solid) and (c,d) fluctuations r^ε about the mean $C^{(0)}$ at small $\mathrm{Pe} = \varepsilon^2$ for uniformly random (a,c) and normally-perturbed periodic ($\sigma = 0.5\varepsilon$) (b,d) sink distributions (for $\varepsilon = 0.1$, $\mathrm{Da} = 2\varepsilon^2$ (a,b) and $\varepsilon = 0.01$, $\mathrm{Da} = \varepsilon\mathrm{Pe}$ (c,d)). Sinks in (a,b) are shown with circles and dashed lines show the homogenization approximation $C^{(0)}$. Dashed lines in (c,d) show the ensemble average $\mathbb{E}[r^\varepsilon]$ from $N_{\mathrm{ens}} = 5\times10^4$ samples, dotted lines show the mean $\pm$ two standard deviations (scaled by $\varepsilon^{-1/2}q^{-1}$).

variance $\sigma_0^2 \equiv (\sigma/\varepsilon)^2$.

In order to assess the magnitude of the difference (2.5) between the homogenized $C^{(0)}(X)$ and exact C solutions to the original problem (2.1), we define the following deterministic measures for a single realisation of r^ε:

$$\|r^\varepsilon\|_C = \max_{X\in[0,1]} |r^\varepsilon|\,, \quad \|r^\varepsilon\|_{L_2}^2 = \int_0^1 (r^\varepsilon)^2\,\mathrm{d}X\,, \quad \|r^\varepsilon\|_{H^1}^2 = \|r^\varepsilon\|_{L_2}^2 + \left\| \frac{\mathrm{d}r^\varepsilon}{\mathrm{d}X} \right\|_{L_2}^2 . \tag{2.6}$$

These are, respectively, the supremum (Chebyshev), mean-squared (L_2) and Sobolev (H^1) norms.

The modes of convergence of C to $C^{(0)}$ defined in (2.6) are arranged in the descending order with respect to their "strength" (except for the Sobolev norm), e.g. $\|r^\varepsilon\|_C \to 0$ as $\varepsilon \to 0$ implies the convergence of $\|r^\varepsilon\|_{L_2}$, while the converse is generally not true. Convergence in the Sobolev norm, which takes account of the first derivative, is stronger than convergence in the mean-squared norm in a sense that $\|\cdot\|_{L_2} \leqslant \|\cdot\|_{H^1}$ (see, e.g. Pavliotis & Stuart (2008) for a more systematic discussion).

3. Correlation properties of the homogenization residue

Panels (c,d) in Figs 3 and 4 summarise the statistical properties of the homogenization residue r^ε by plotting an individual realisation of $r^\varepsilon(\mathrm{X})$ (solid line) together with a pointwise 95%-confidence interval (± 2 standard errors SE=$(\mathbb{V}\mathrm{ar}[r^\varepsilon]/N_{\mathrm{ens}})^{1/2}$; dotted lines) and the pointwise ensemble mean $\mathbb{E}[r^\varepsilon]$ (dashed lines) computed via Monte-Carlo simulations of (2.1) for an ensemble of N_{ens} realisations. We note a very different spatial structure of the residue for f_n (Fig. 3d) as compared to f_u (Fig. 3c) at large Pe (CLDJ); moreover, despite a more "smooth" appearance of fluctuations at small Pe, their magnitude in the case of f_u (Fig. 4c) is much larger (over 20-fold for $\sigma = 0.5\varepsilon$, $\mathrm{Pe} = \varepsilon^2$, $\varepsilon = 0.01$) than for f_n (Fig. 4d).

To study the spatial correlation of the homogenization residue r^ε in more detail, in addition to pointwise variance $\mathbb{V}\mathrm{ar}[r^\varepsilon(X)]$ and covariance $\mathbb{C}\mathrm{ov}(r^\varepsilon(X), r^\varepsilon(Y))$, we adopt the *transverse covariance*

$$\mathbb{C}\mathrm{ov}_{\mathrm{T}}(r^\varepsilon) \equiv \mathbb{C}\mathrm{ov}(r^\varepsilon(X), r^\varepsilon(1-X)) = \mathbb{E}\big[\,(r^\varepsilon(X) - \mathbb{E}[r^\varepsilon(X)])\,(r^\varepsilon(1-X) - \mathbb{E}[r^\varepsilon(1-X)])\,\big], \tag{3.1}$$

which characterises to some degree how fluctuations are correlated across the domain.

3.1. *Numerical estimates of the covariance of the homogenization residue*

Covariance matrices for the fluctuations in solute concentration about the mean at small Pe, computed on a uniformly random array (Fig. 5c) and on a normally-perturbed periodic array (Fig. 5d), show a prominent cloud about the main diagonal, giving evidence for long-range spatial correlations (illustrated by the pointwise variance and transverse covariance distributions in Figs 5(a) and 5(b) respectively, analogues of the confidence intervals in Fig. 4(c,d)). The computed variances and transverse covariances for f_u, f_n are in a good agreement with theoretical predictions, which will be obtained below.

In addition to the advection-dominated case ($\mathrm{Pe} \gg 1$), illustrated in Fig. 3 (see also Fig. 4 of CLDJ), we further investigate the correlation properties by considering the case when advection and diffusion balance over the inter-sink distance ($\mathrm{Pe} = O(1)$): illustrated in Figure 6. For the normally-perturbed distribution f_n we observe a marked advection-induced drop in the transverse covariance (Fig. 6b) and a very narrow band about the main diagonal of the covariance matrix (Fig. 6d), indicating a greater independence of each unit cell in the case of f_n as compared to f_u. The variance, like the pointwise standard deviation in Fig. 4(d), is uniform across the domain (outside the boundary layers at $X = 0, 1$) for f_n but varies much more smoothly for f_u (Fig. 6(a,c)). It is also of interest to note the negative correlation (or "anti-correlation") in fluctuations at the points symmetrical about the centre of the array and close to the boundaries for f_u (Fig. 5a) but not for f_n (Fig. 5b) at small Pe. As Péclet number increases, however, this feature gradually disappears (Fig. 6a).

It is also interesting to highlight that the parabolic variance and transverse covariance of the residue for a normally-perturbed array at small Pe (Fig. 5b) closely resemble the shape of $\mathbb{V}\mathrm{ar}[r^\varepsilon]$ and $\mathbb{C}\mathrm{ov}_{\mathrm{T}}[r^\varepsilon]$ for a uniformly-random array for moderate-to-large Pe (Fig. 6(a) and Fig. 4(d,e) of CLDJ); In the following Sections, we seek to explore analytically how features such as the boundary layers in Fig. 6(b), indicated by Monte-Carlo simulations, arise from the interaction of deterministic and stochastic factors in transport past an array of sinks. Motivated by the structure of parameter space (Fig. 1a), we consider the structure of

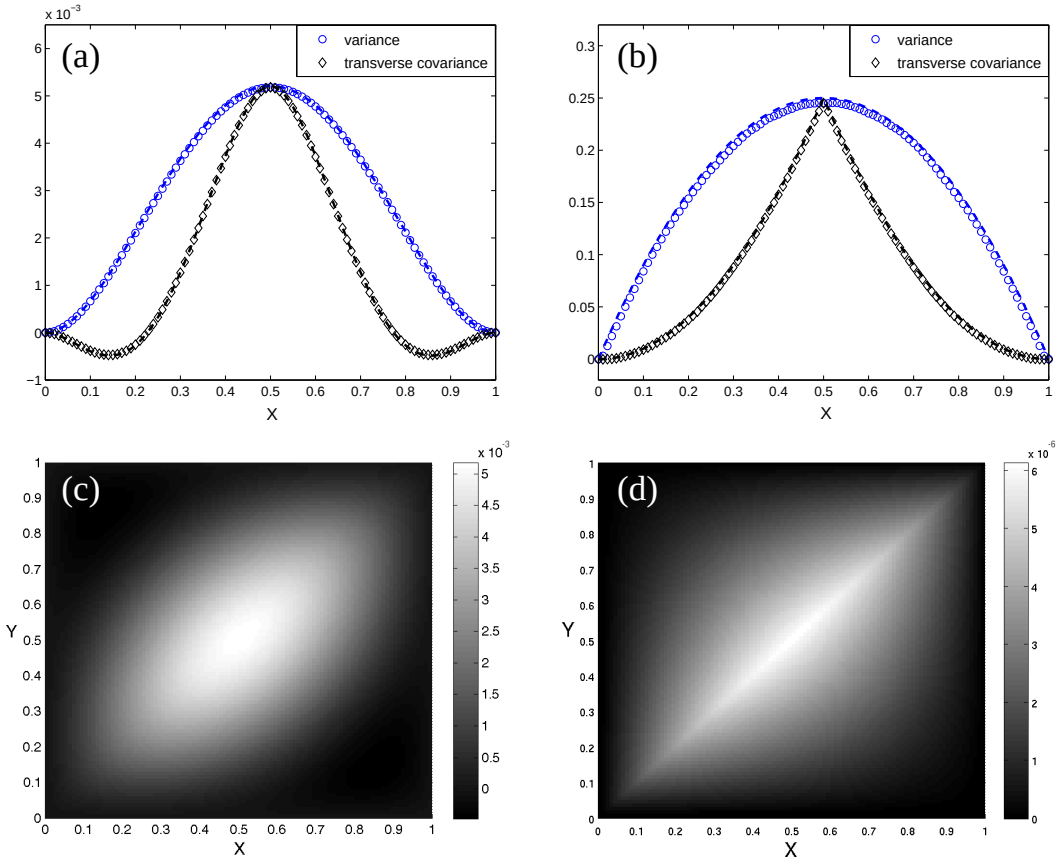

Figure 5. Statistical properties of the homogenization residue for a uniformly random (a,c) and normally-perturbed (b,d) periodic array at small Péclet number ($\mathrm{Pe} = \varepsilon^2$, $\mathrm{Da} = \varepsilon\mathrm{Pe}$, $\varepsilon = 0.01$). (a,b) Spatial distribution of the pointwise variance $\mathbb{V}\mathrm{ar}[r^\varepsilon]$ (circles) and transverse covariance $\mathbb{C}\mathrm{ov}(r^\varepsilon(X), r^\varepsilon(1-X))$ (diamonds) of the homogenization residue r^ε computed for an ensemble of size $N_{\mathrm{ens}} = 5\times 10^4$, and corresponding theoretical predictions (dashed lines) (3.18) and (3.19) for uniformly random (scaled by $(\varepsilon q^2)^{-1}$) (a) and (3.13) and (3.14) for normally-perturbed array with $\sigma_0 \equiv \sigma/\varepsilon = 0.5$ (scaled by $(\varepsilon^3 q^2 \sigma_0^2)^{-1}$) (b). (c,d) Covariance matrix $\mathbb{C}\mathrm{ov}(r^\varepsilon(X), r^\varepsilon(Y))$ corresponding to (a,b), computed at 100 equispaced points and scaled by $1/(\varepsilon q^2)$ ($q = \varepsilon^{-2}\mathrm{Da}$).

multiscale fluctuations of the residue r^ε at the two organising centres: (i) $\mathrm{Pe} = O(\varepsilon)$, $\mathrm{Da} = O(\varepsilon^2)$ in § 3.2 and (ii) $\mathrm{Pe} = O(1)$, $\mathrm{Da} = O(\varepsilon)$ in § 3.3.

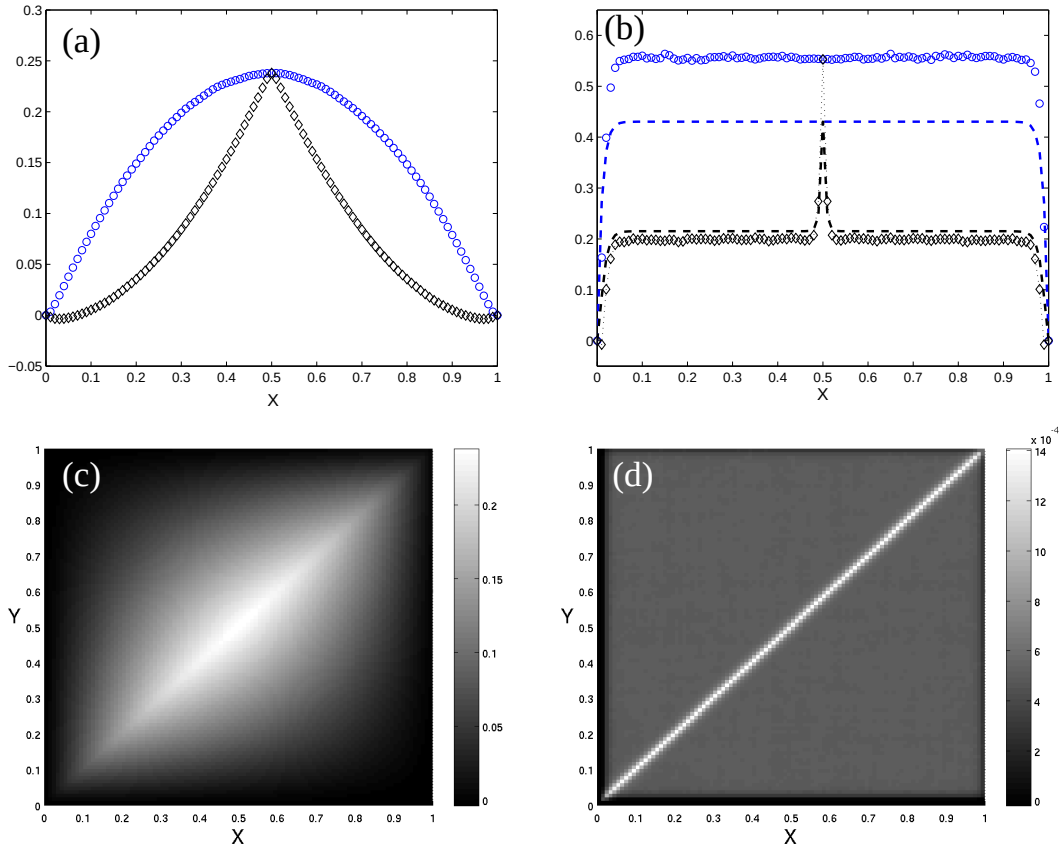

Figure 6. Statistical properties of the homogenization residue for a uniformly random (a,c) and normally-perturbed (with $\sigma = 0.5\varepsilon$) (b,d) periodic array at moderate Péclet number (Pe $= 1$, Da $= \varepsilon$Pe, $\varepsilon = 0.01$). (a,b) Spatial distribution of the pointwise variance $\mathbb{V}\mathrm{ar}[r^\varepsilon]$ (circles) and transverse covariance $\mathbb{C}\mathrm{ov}_\mathrm{T}(r^\varepsilon)$ (diamonds); dashed lines in (b) indicate theoretical predictions (3.36) and (3.37) scaled by $(\varepsilon q_1 \sigma_0)^{-2}$ ($q_1 = \varepsilon^{-1}$Da). (c,d) Covariance matrix $\mathbb{C}\mathrm{ov}(r^\varepsilon(X), r^\varepsilon(Y))$ corresponding to (a,b) (computed at 100 equispaced points, using 5×10^4 realisations; all plots except for (b) are scaled by ε^{-1}).

3.2. *Analytical estimates of covariance for* Pe $= O(\varepsilon)$, Da $= O(\varepsilon^2)$ *(diffusion-dominated at the inter-sink scale)*

We start by briefly recalling (and also extending) the method introduced in CLDJ for finding a correction to the leading order solution $C^{(0)}$ in the case of uniformly-random or normally-perturbed sink distributions for Pe $= O(\varepsilon)$, Da $= O(\varepsilon^2)$ (again writing Pe $= \varepsilon p$ and Da $= \varepsilon^2 q$). By using the statistical properties of these distributions and an exact solution for a cell problem, we can estimate analytically the mean and covariance of the homogenization residue.

When sinks are distributed non-periodically we can derive the homogenized approximation of (2.1) as

follows. We initially use (2.2) to rewrite (2.1) as

$$\begin{aligned} &C_{xx}+2\varepsilon C_{xX}+\varepsilon^2 C_{XX}-\varepsilon p\,(C_x+\varepsilon C_X)=\varepsilon^2 q\,f, \quad (0<x<\varepsilon^{-1}, 0<X<1),\\ &C|_{X=0}=1, \quad C|_{X=1}=0. \end{aligned} \tag{3.2}$$

(assuming here for brevity that C does not fall to zero upstream of $X=1$). We allow $C^{(1)}$, $C^{(2)}$, ... to have fluctuations, assuming that these are not large enough to disrupt the proposed expansion. At leading order, $C^{(0)}_{xx}=0$, $C^{(0)}|_{X=0}=1$ and $C^{(0)}|_{X=1}=0$. Thus $C^{(0)}(x,X)=\tilde{A}(X)x+\tilde{B}(X)$. The first term must be suppressed to avoid secular growth, so that $C^{(0)}=C^{(0)}(X)$. Likewise at the following order we find that $C^{(1)}=C^{(1)}(X)$. Collecting the terms in (3.2) at $O(\varepsilon^2)$, we obtain

$$C^{(2)}_{xx}=q(f-F), \quad \text{where} \quad qF(X)\equiv C^{(0)}_{XX}-pC^{(0)}_X, \tag{3.3}$$

with $f=\sum_{i=1}^{N}\delta(x-\xi_i)$. This is to be solved subject to $C^{(1)}=C^{(2)}=0$ at $x=0$ and $x=\varepsilon^{-1}$. Thus in $\xi_i<x<\xi_{i+1}$ $(i=0,1,\ldots,N)$, treating x and X as independent and assuming F is independent of i to leading order (verified *a posteriori*), we have

$$C^{(2)}=-\tfrac{1}{2}qF(x-\xi_i)^2+\alpha_i(x-\xi_i)+\beta_i \tag{3.4}$$

for some α_i, β_i, taking $\xi_0=0$ and $\xi_{N+1}=\varepsilon^{-1}$.

Using the diffusive-uptake flux balance in (3.3) at each sink and applying the global boundary conditions $C^{(2)}|_{x=0}=C^{(2)}|_{x=\varepsilon^{-1}}=0$, we can derive recurrence relations for α_i and β_i, which after some manipulation, lead to the explicit expression (see Appendix B in CLDJ for more detail)

$$C^{(2)}=\tfrac{1}{2}qF\,x(\varepsilon^{-1}-x)+q\left[(\varepsilon xR_N-R_i)+x(i-N)\right], \quad i=1,2,\ldots,N \quad \text{for} \quad \xi_i<x<\xi_{i+1}, \tag{3.5}$$

where

$$R_i=\sum_{j=1}^{i}\xi_j \tag{3.6}$$

is a linear functional (partial sum) of the random sink positions. Expression (3.5) thus relates solute fluctuations directly to sink distributions.

We note that all terms except $\varepsilon xR_N-R_i\equiv XR_N-R_i$ (setting $x=X/\varepsilon$) in (3.5) are deterministic, and therefore

$$C^{(2)}-\mathbb{E}[C^{(2)}]=q\,(X\mathring{R}_N-\mathring{R}_i), \tag{3.7}$$

where $\mathring{R}_i\equiv R_i-\mathbb{E}[R_i]$, and $i\in\{1,\ldots,N\}$ satisfies $\xi_i<x<\xi_{i+1}$.

Likewise $\mathbb{C}\mathrm{ov}(C^{(2)}(X),C^{(2)}(Y))=q^2\,\mathbb{C}\mathrm{ov}\big(XR_N-R_i,YR_N-R_k)\big)$, (where $i,k\in\{1,\ldots,N\}$ satisfies $i=\lfloor\varepsilon^{-1}X\rfloor$, $k=\lfloor\varepsilon^{-1}Y\rfloor$), so that

$$\mathbb{C}\mathrm{ov}(C^{(2)}(X),C^{(2)}(1-X))\simeq q^2\,\mathbb{C}\mathrm{ov}\big(XR_N-R_i,(1-X)R_N-R_{N-i}\big). \tag{3.8}$$

The choice of $N-i$ instead of $N+1-i$ does not affect the results at leading-order, owing to large $N\gg 1$ and the smooth X-dependence of the variance and the transverse covariance, as will be shown below.

Thus, by applying the definition (3.1) to (3.7) and (3.8), the variance and the transverse covariance of the correction are expressed in terms of the partial sums R_i (3.6) for $i = \lfloor \varepsilon^{-1} X \rfloor$ as follows:

$$\mathbb{V}\mathrm{ar}[C^{(2)}] = q^2\, \mathbb{E}\big[(X\mathring{R}_N - \mathring{R}_i)^2\big] = q^2 \left\{X^2 \mathbb{V}\mathrm{ar}[R_N] - 2X\mathbb{C}\mathrm{ov}(R_i, R_N) + \mathbb{V}\mathrm{ar}[R_i]\right\}, \tag{3.9a}$$

$$\begin{aligned}\mathbb{C}\mathrm{ov}_{\mathrm{T}}[C^{(2)}] &= q^2\, \mathbb{E}\big[\{X\mathring{R}_N - \mathring{R}_i\}\{(1-X)\mathring{R}_N - \mathring{R}_{N-i}\}\big] = \\ &= q^2 \big\{X(1-X)\mathbb{V}\mathrm{ar}[R_N] - (1-X)\mathbb{C}\mathrm{ov}(R_i, R_N) - X\mathbb{C}\mathrm{ov}(R_{N-i}, R_N) + \\ &\qquad + \mathbb{C}\mathrm{ov}(R_i, R_{N-i})\big\}.\end{aligned} \tag{3.9b}$$

Our task therefore reduces to finding the corresponding variances and covariances of the partial sums R_i (3.6) for specific sink distributions.

3.2.1. Normally-perturbed sinks

Recall when $f = f_n$, we have $\xi_i \sim \mathcal{N}(i, \sigma_0^2)$. From (B.1) and (B.2), given in Appendix B, the mean, variance and covariance of R_i can be expressed as

$$\mathbb{E}[R_i] = \frac{i(i+1)}{2}, \quad \mathbb{V}\mathrm{ar}[R_i] = \mathbb{C}\mathrm{ov}(R_i, R_k) = i\,\sigma_0^2, \quad (i \leqslant k), \tag{3.10}$$

and thus (3.9) simplifies to

$$\mathbb{V}\mathrm{ar}[C^{(2)}] = q^2 \left\{X^2 \mathbb{V}\mathrm{ar}[R_N] + (1-2X)\mathbb{V}\mathrm{ar}[R_i]\right\}, \qquad (X < 1,\ i = \lfloor \varepsilon^{-1} X \rfloor \leqslant N), \tag{3.11a}$$

$$\mathbb{C}\mathrm{ov}_{\mathrm{T}}[C^{(2)}] = q^2 \left\{X(1-X)\mathbb{V}\mathrm{ar}[R_N] + X\,\mathbb{V}\mathrm{ar}[R_i] - X\,\mathbb{V}\mathrm{ar}[R_{N-i}]\right\}, \quad (X < \tfrac{1}{2},\ i \leqslant \tfrac{N}{2}). \tag{3.11b}$$

By setting $i = (i-x) + \varepsilon^{-1}X$ and $N = \varepsilon^{-1} - 1$, we obtain from (3.10), $\mathbb{E}[XR_N - R_i] = \varepsilon^{-2}\frac{1}{2}X(1-X) - \frac{1}{2}(x+i)(i+1-x)$. Substituting this into (3.5), we get an expectation of the correction in the case of normal perturbations (CLDJ):

$$\mathbb{E}(C^{(2)}) = \varepsilon^{-2}\,\tfrac{1}{2}\,q\,(F-1)X(1-X) + \tfrac{1}{2}\,q\,(x-i)(i+1-x). \tag{3.12}$$

To ensure the original expansion is asymptotic, we must take $F = 1$ at $O(\varepsilon^{-2})$, yielding from (3.3) the leading-order equation for $C^{(0)}$ and recovering the parabolic cell solution obtained in CLDJ for a periodic array. Simulations indicate that the contribution at $O(\varepsilon^{-1})$ (and hence $C^{(1)}$) vanishes; however, a further correction to $\mathbb{E}[r^{\varepsilon}]$ of the order of ε^2 is present, presumably involving a closure condition for the correction at higher order.

Substituting the variance and covariance of the partial sums R_i (3.10) into (3.11), setting $i = \varepsilon^{-1}X + \gamma$ ($\gamma \equiv i - x = O(1)$) and $N = \varepsilon^{-1} - 1$, and retaining the leading-order term in powers of ε, we find, after some algebra, that (3.11a) gives, for the variance (CLDJ),

$$\mathbb{V}\mathrm{ar}[C^{(2)}] = \varepsilon^{-1}\,q^2\,\sigma_0^2\,X(1-X) + O(1), \tag{3.13}$$

and using (3.11b) for $0 \leqslant X \leqslant \frac{1}{2}$, $i \leqslant N-i$ (owing to the symmetry of the covariance) gives, for the transverse covariance (not reported previously),

$$\mathbb{C}\mathrm{ov}_{\mathrm{T}}[C^{(2)}] = \begin{cases} \varepsilon^{-1} q^2 \sigma_0^2 X^2 + O(1), & 0 \leqslant X \leqslant \frac{1}{2}, \\ \varepsilon^{-1} q^2 \sigma_0^2 (1-X)^2 + O(1), & \frac{1}{2} < X \leqslant 1, \end{cases} \tag{3.14}$$

in a good agreement with simulations (Fig. 5b). From (2.6), (3.12) and (3.13), we have $\|\mathbb{E}[C^{(2)}]\|_C = \frac{1}{8} q$, $\|\mathbb{E}[C^{(2)}]\|_{L_2} = \frac{\sqrt{30}}{60} q$, $\|\mathbb{E}[C^{(2)}]\|_{H^1} = \frac{\sqrt{3}}{6} \varepsilon^{-1} q \sqrt{1 + \frac{1}{10}\varepsilon^2}$, (where we integrate over $(i, i+1)$ and use $\mathrm{d}/\mathrm{d}X = \varepsilon^{-1}\mathrm{d}/\mathrm{d}x$), and $\|\mathbb{V}\mathrm{ar}[C^{(2)}]\|_C \approx \frac{1}{4} \varepsilon^{-1} q^2 \sigma_0^2$, $\|\mathbb{V}\mathrm{ar}[C^{(2)}]\|_{L_2} \approx \frac{\sqrt{30}}{30} \varepsilon^{-1} q^2 \sigma_0^2$, $\|\mathbb{V}\mathrm{ar}[C^{(2)}]\|_{H^1} \approx \frac{\sqrt{330}}{30} \varepsilon^{-1} q^2 \sigma_0^2$, so that $\|\cdot\|_{L_2} \leqslant \|\cdot\|_C \leqslant \|\cdot\|_{H^1}$, as expected. We estimate the magnitude of the homogenization residue as

$$\|r^\varepsilon\| \approx \varepsilon^2 \left(\|\mathbb{E}[C^{(2)}]\| + \|\mathbb{V}\mathrm{ar}[C^{(2)}]\|^{1/2} \right), \tag{3.15}$$

for each of these norms, and hence

$$\|r^\varepsilon\|_C = \|r^\varepsilon\|_{L_2} = O(q \sigma_0 \varepsilon^{3/2}), \quad \|r^\varepsilon\|_{H^1} = O(q\varepsilon). \tag{3.16}$$

Thus while $C^{(2)}$ has $O(1)$ mean, r^ε is dominated by fluctuations of relative magnitude $O(\varepsilon^{3/2})$; however the gradients in $\mathbb{E}[r^\varepsilon]$ are larger than the fluctuations about the mean (the large gradients at the inter-sink scale of $C^{(2)}$, which contribute to slower convergence in the Sobolev norm than in the mean-squared norm, are illustrated in Fig. 4d). This approximation holds as long as sinks do not exchange places, which can be expected once σ_0 becomes sufficiently large. Because $\mathbb{V}\mathrm{ar}[C^{(2)}]$ scales with σ_0, (3.13) suggests that the fluctuations in the case of stronger mixing of perturbed sink locations will be larger than $O(\varepsilon^{3/2})$.

3.2.2. Uniformly random sinks

For $f = f_u$, the sinks form order statistics with the inter-sink distances obeying a Dirichlet distribution of dimension $N+1$ (Matsunawa, 1985) (see Appendix B for more detail).

From the properties of the linear combination of the order statistics (B.15), we have

$$\mathbb{V}\mathrm{ar}[R_i] = \frac{i(i+1)(2i+1)(N+1)}{6(N+2)} - \frac{(\mathbb{E}[R_i])^2}{N+2}, \quad \mathbb{E}[R_i] = \frac{i(i+1)}{2}, \tag{3.17a}$$

$$\mathbb{C}\mathrm{ov}(R_i, R_k) = \frac{i(i+1)(2i+1)(N+1)}{6(N+2)} + \frac{i(i+1)(k-i)(N+1)}{2(N+2)} - \frac{\mathbb{E}[R_i]\,\mathbb{E}[R_k]}{N+2}, \quad i \leqslant k. \tag{3.17b}$$

Substituting (3.17) into (3.9) and again writing $i = \varepsilon^{-1}X + (i-x)$ (taking $|i-x| = O(1)$), we find to leading order in ε (using `Maple`) explicit expressions for the variance (as in CLDJ) and the transverse covariance (which has not been reported previously) of the correction in the case of a uniformly random sink distribution:

$$\mathbb{V}\mathrm{ar}[C^{(2)}] = \varepsilon^{-3} q^2 \tfrac{1}{12} X^2 (1-X)^2 + O(\varepsilon^{-2}), \tag{3.18}$$

$$\mathbb{C}\mathrm{ov}_{\mathrm{T}}[C^{(2)}] = \begin{cases} -\varepsilon^{-3} q^2 \, \frac{1}{12} X^2 (1 - 6X + 7X^2) + O(\varepsilon^{-2}), & 0 \leqslant X \leqslant \frac{1}{2}, \\ -\varepsilon^{-3} q^2 \, \frac{1}{12} (1-X)^2 (2 - 8X + 7X^2) + O(\varepsilon^{-2}), & \frac{1}{2} < X \leqslant 1, \end{cases} \tag{3.19}$$

which are in a good agreement with numerical solutions shown in Figure 5(a).

From (2.6) and (3.18), we find $\|\mathbb{V}\mathrm{ar}[C^{(2)}]\|_C \approx \frac{1}{192}\,\varepsilon^{-3} q^2$, $\|\mathbb{V}\mathrm{ar}[C^{(2)}]\|_{L_2} \approx \frac{\sqrt{70}}{2520}\,\varepsilon^{-3} q^2$, $\|\mathbb{V}\mathrm{ar}[C^{(2)}]\|_{H^1} \approx \frac{\sqrt{910}}{2520}\,\varepsilon^{-3} q^2$, (with $\|\mathbb{E}[C^{(2)}]\|_C = \|\mathbb{E}[C^{(2)}]\|_{L_2} = O(q)$, $\|\mathbb{E}[C^{(2)}]\|_{H^1} = O(\varepsilon^{-1} q)$, as for the f_n distribution). Therefore, using (3.15), we have

$$\|r^\varepsilon\|_C = \|r^\varepsilon\|_{L_2} = \|r^\varepsilon\|_{H^1} = O(q\,\varepsilon^{1/2}). \tag{3.20}$$

The fluctuations about $C^{(0)}$ are thus $O(\varepsilon^{1/2})$, which is significantly larger than the $O(\varepsilon^2)$ error for the magnitude of homogenization on periodic arrays (CLDJ), and they even dominate $O(\varepsilon)$ contribution of the gradients in the mean (periodic) component of r^ε. (Fig. 4(c,d) shows how the homogenization residue with $f = f_u$ varies more smoothly at the inter-sink scale than the residue with $f = f_n$.)

We complete the analysis by considering the fluctuations in a homogenization residue about the second organising centre $\mathrm{Pe} = O(1)$, $\mathrm{Da} = O(\varepsilon)$.

3.3. *Analytical estimates of covariance for* $\mathrm{Pe} = O(1)$, $\mathrm{Da} = O(\varepsilon)$ *(balanced advection-diffusion at the inter-sink scale)*

It remains to establish the statistical properties of the homogenization residue in the case of moderate-to-large local Péclet numbers $\mathrm{Pe} = O(1)$, $\mathrm{Da} = O(\varepsilon) = \varepsilon q_1$, $q_1 = O(1)$), when (2.1) transforms to the following problem:

$$\begin{aligned} &C_{xx} + 2\varepsilon C_{xX} + \varepsilon^2 C_{XX} - \mathrm{Pe}\,(C_x + \varepsilon C_X) = \varepsilon q_1 f, \quad f = \sum_{i=1}^{N} \delta(x - \xi_i) \\ &C|_{X=0} = 1, \quad C|_{X=1} = 0 \end{aligned} \tag{3.21}$$

(again assuming here, without loss of generality, that C does not fall to zero upstream of $X = 1$). At $O(1)$, we get $C^{(0)}_{xx} - \mathrm{Pe}\,C^{(0)}_x = 0$, $C^{(0)}|_{X=0} = 1$ and $C^{(0)}|_{X=1} = 0$. Thus $C^{(0)}(x,X) = \tilde{a}(X)\mathrm{e}^{Pex} + \tilde{b}(X)$, $\tilde{a}, \tilde{b}$ being arbitrary constants of X. The first term must be suppressed to avoid secular growth (since $x = \varepsilon^{-1} \to \infty$ as $\varepsilon \to 0$), so that again $C^{(0)} = C^{(0)}(X)$.

Collecting the terms in (3.21) at $O(\varepsilon)$, we obtain

$$C^{(1)}_{xx} - \mathrm{Pe}\,C^{(1)}_x = q_1(f(x) - F(X)), \quad \text{where} \quad q_1 F(X) \equiv -\mathrm{Pe}\,C^{(0)}_X. \tag{3.22}$$

This is to be solved between each pair of sinks ξ_i and ξ_{i+1} ($i = 0, \ldots, N$, taking again $\xi_0 = 0$ and $\xi_{N+1} = \varepsilon^{-1}$), subject to $C^{(1)} = 0$ at $x = 0$ and $x = \varepsilon^{-1}$. Thus

$$C^{(2)} = \tfrac{q_1}{\mathrm{Pe}} F(x - \xi_i) + \tilde{\alpha}_i \mathrm{e}^{\mathrm{Pe}(x - \xi_i)} + \tilde{\beta}_i, \quad \xi_i < x < \xi_{i+1} \ \text{ for } i = 0, \ldots, N, \tag{3.23}$$

with some $\tilde{\alpha}_i$, $\tilde{\beta}_i$ to be determined.

Integrating (3.22) across $x = \xi_i$ gives the balance of concentrations and fluxes: $C^{(1)}|_{\xi_i+} = C^{(1)}|_{\xi_i-}$ and $C^{(1)}_x|_{\xi_i+} - C^{(1)}_x|_{\xi_i-} = q_1$, which (using (3.23) for $\xi_i < x < \xi_{i+1}$ and $\xi_{i-1} < x < \xi_i$) allows us to obtain the

following recurrence relations:

$$\tilde{\alpha}_i = \tilde{\alpha}_{i-1}\,\mathrm{e}^{\mathrm{Pe}\Delta_i} + \tfrac{q_1}{\mathrm{Pe}}, \tag{3.24a}$$

$$\tilde{\beta}_i = \tilde{\beta}_{i-1} + \tfrac{q_1}{\mathrm{Pe}}(F\,\Delta_i - 1)\,, \tag{3.24b}$$

where $\Delta_i = \xi_i - \xi_{i-1}$, for $i = 1, 2, \ldots, N$.

Summing (3.24b), taking the product of (3.24a) for $j = 1, 2, \ldots, i,$ and assuming that F is independent of i to leading order, we find

$$\tilde{\alpha}_i = \mathrm{e}^{\mathrm{Pe}\,\xi_i}\Big(\tilde{\alpha}_0 + \tfrac{q_1}{\mathrm{Pe}}\sum_{j=1}^{i}\mathrm{e}^{-\mathrm{Pe}\,\xi_j}\Big), \tag{3.25a}$$

$$\tilde{\beta}_i = \tilde{\beta}_0 + \tfrac{q_1}{\mathrm{Pe}}\,(F\,\xi_i - i)\,, \tag{3.25b}$$

using the identity $\sum_{j=1}^{i}\Delta_j \equiv \xi_i$.

We define

$$Q_i \equiv \sum_{j=1}^{i}\mathrm{e}^{-\mathrm{Pe}\,\xi_j} \tag{3.26}$$

and substitute (3.25) into (3.23) to find

$$C^{(1)} = \tfrac{q_1}{\mathrm{Pe}}\,(Fx - i) + \big(\tilde{\alpha}_0 + \tfrac{q_1}{\mathrm{Pe}}\,Q_i\big)\,\mathrm{e}^{\mathrm{Pe}\,x} + \tilde{\beta}_0 \quad \xi_i < x < \xi_{i+1},\ i = 0, \ldots, N\,. \tag{3.27}$$

Imposing $C^{(2)} = 0$ at $x = 0$ $(i = 0)$ and $x = \varepsilon^{-1}$ $(i = N)$ to satisfy the global boundary conditions, gives $\tilde{\alpha}_0 = -\tilde{\beta}_0 = -\frac{q_1}{\mathrm{Pe}}\,[F\varepsilon^{-1} - N + Q_N\,\mathrm{e}^{\mathrm{Pe}\,\varepsilon^{-1}}]/(\mathrm{e}^{\mathrm{Pe}\,\varepsilon^{-1}} - 1)$, and so, after some algebra, we obtain

$$\begin{aligned} C^{(1)} \;=\; & \frac{q_1}{\mathrm{Pe}}\left[(Fx - i) - (F\varepsilon^{-1} - N)\,\frac{\mathrm{e}^{\mathrm{Pe}\,x} - 1}{\mathrm{e}^{\mathrm{Pe}/\varepsilon} - 1}\right] - \\ & - \frac{q_1/Pe}{1 - \mathrm{e}^{-\mathrm{Pe}/\varepsilon}}\left[(\mathrm{e}^{\mathrm{Pe}\,x} - 1)\,Q_N - \mathrm{e}^{\mathrm{Pe}\,x}(1 - \mathrm{e}^{-\mathrm{Pe}/\varepsilon})\,Q_i\right], \quad \xi_i < x < \xi_{i+1},\ i = 0, \ldots, N. \end{aligned} \tag{3.28}$$

This expression again relates solute fluctuations directly to sink distributions and is the analogue of (3.5).

Analogously to § 3.2, we observe that the statistical properties of the correction $C^{(1)}$, and thus the homogenization residue $r^\varepsilon \approx C - C^{(1)}$, are entirely defined by the combination of exponential partial sums Q_i and Q_N in the second term of (3.28). Therefore (setting $x = X/\varepsilon$) in (3.5), we have

$$C^{(1)} - \mathbb{E}[C^{(1)}] = -\frac{q_1/Pe}{1 - \mathrm{e}^{-\mathrm{Pe}/\varepsilon}}\left[(\mathrm{e}^{\mathrm{Pe}\,X/\varepsilon} - 1)\,\mathring{Q}_N - \mathrm{e}^{\mathrm{Pe}\,X/\varepsilon}(1 - \mathrm{e}^{-\mathrm{Pe}/\varepsilon})\,\mathring{Q}_i\right], \tag{3.29}$$

where $\mathring{Q}_i \equiv Q_i - \mathbb{E}[Q_i],\ i = 1, \ldots, N$.

Applying the definition of variance and transverse covariance (3.1) to (3.29), expanding and taking the expectation, we express $\mathbb{V}\mathrm{ar}[C^{(1)}]$ and $\mathbb{C}\mathrm{ov}_{\mathrm{T}}[C^{(1)}]$ in terms of the partial sums Q_i of a sink distribution ξ_i as

follows:

$$\begin{aligned}\mathbb{V}\mathrm{ar}[C^{(1)}] &= \left(\tfrac{q_1/Pe}{1-\mathrm{e}^{-\mathrm{Pe}/\varepsilon}}\right)^2 \mathbb{E}\left[\left\{(\mathrm{e}^{\mathrm{Pe}X/\varepsilon}-1)\,\mathring{Q}_N - \mathrm{e}^{\mathrm{Pe}X/\varepsilon}(1-\mathrm{e}^{-\mathrm{Pe}/\varepsilon})\,\mathring{Q}_i\right\}^2\right] \\ &= \left(\tfrac{q_1/Pe}{1-\mathrm{e}^{-\mathrm{Pe}/\varepsilon}}\right)^2 \left\{\left(\mathrm{e}^{\mathrm{Pe}X/\varepsilon}-1\right)^2 \mathbb{V}\mathrm{ar}[Q_N] - \right. \\ &\left. -2\mathrm{e}^{\mathrm{Pe}X/\varepsilon}\left(\mathrm{e}^{\mathrm{Pe}X/\varepsilon}-1\right)\left(1-\mathrm{e}^{-\mathrm{Pe}/\varepsilon}\right)\mathbb{C}\mathrm{ov}(Q_i,Q_N) + \mathrm{e}^{2\mathrm{Pe}X/\varepsilon}\left(1-\mathrm{e}^{-\mathrm{Pe}/\varepsilon}\right)^2 \mathbb{V}\mathrm{ar}[Q_i]\right\},\end{aligned} \tag{3.30}$$

$$\begin{aligned}\mathbb{C}\mathrm{ov}_{\mathrm{T}}[C^{(1)}] &= \left(\tfrac{q_1}{\eta\,\mathrm{Pe}}\right)^2 \mathbb{E}\left[\left\{(\mathrm{e}^{\mathrm{Pe}X/\varepsilon}-1)\,\mathring{Q}_N - \eta\,\mathrm{e}^{\mathrm{Pe}X/\varepsilon}\,\mathring{Q}_i\right\}\right. \\ &\qquad \left.\left\{(\mathrm{e}^{\mathrm{Pe}(1-X)/\varepsilon}-1)\,\mathring{Q}_N - \eta\,\mathrm{e}^{\mathrm{Pe}(1-X)/\varepsilon}\,\mathring{Q}_{N-i}\right\}\right] = \\ &= \left(\tfrac{q_1}{\eta\,\mathrm{Pe}}\right)^2 \left\{\left(1-\mathrm{e}^{\mathrm{Pe}X/\varepsilon}-\mathrm{e}^{\mathrm{Pe}(1-X)/\varepsilon}+\mathrm{e}^{\mathrm{Pe}/\varepsilon}\right)\mathbb{V}\mathrm{ar}[Q_N] + \right. \\ &+\eta\left(\mathrm{e}^{\mathrm{Pe}X/\varepsilon}-\mathrm{e}^{\mathrm{Pe}/\varepsilon}\right)\mathbb{C}\mathrm{ov}(Q_i,Q_N) + \eta\left(\mathrm{e}^{\mathrm{Pe}(1-X)/\varepsilon}-\mathrm{e}^{\mathrm{Pe}/\varepsilon}\right)\mathbb{C}\mathrm{ov}(Q_{N-i},Q_N) + \\ &\left.+\eta^2\mathrm{e}^{\mathrm{Pe}/\varepsilon}\,\mathbb{C}\mathrm{ov}(Q_i,Q_{N-i})\right\},\end{aligned} \tag{3.31}$$

where $\eta \equiv 1-\mathrm{e}^{-\mathrm{Pe}/\varepsilon}$.

Our task once again to find the corresponding variances and covariances of the partial sum Q_i for a specific sink distribution. However, in this case, the functional of the sink distribution (3.26) becomes nonlinear (*cf.* (3.6)) despite the linearity of the original problem (2.1). We pursue this task for normally-perturbed sinks, leaving the uniformly random case for a future study.

3.3.1. Normally-perturbed sink distribution

Consider $f = f_n$, $\xi_i \sim \mathcal{N}(i,\sigma_0^2)$. For $\sigma_0 \equiv \sigma/\varepsilon \ll 1$ and Pe not too large, we can assume $g(\xi_i) \equiv \mathrm{e}^{-\mathrm{Pe}\,\xi_i}$ has an approximately normal distribution, so that expanding it about the mean sink location $\mu_i = i$, we have

$$g(\mu_i + (\xi_i - \mu_i)) \approx g_i + g_i'(\xi_i-\mu_i) + \tfrac{1}{2}g_i''(\xi_i-\mu_i)^2 + \ldots, \quad g_i \equiv g(\mu_i). \tag{3.32}$$

We then compute the approximate mean and variance of $g(\mu_i)$

$$\mathbb{E}[g(\mu_i+(\xi_i-\mu_i))] \approx g_i + \tfrac{1}{2}g_i''\,\mathbb{V}\mathrm{ar}[\xi_i] + \tfrac{1}{24}g_i''''\,\mathbb{E}[(\xi_i-\mu_i)^4] + \ldots, \tag{3.33a}$$

$$\mathbb{V}\mathrm{ar}[g(\xi_i)] \equiv \mathbb{E}[g(\xi_i)^2] - (\mathbb{E}[g(\xi_i)])^2, \tag{3.33b}$$

which, using the moments of the normally-distributed ξ_i, reduces (see Appendix B) to

$$\mathbb{V}\mathrm{ar}[g(\xi_i)] \approx \mathrm{Pe}^2\sigma_0^2\left[1+\tfrac{3}{2}\,\mathrm{Pe}^2\sigma_0^2\right]\mathrm{e}^{-2\mathrm{Pe}\,i}. \tag{3.34}$$

The partial sum (3.26) can be equivalently rewritten as $Q_i \equiv \sum_{j=1}^{i} g(\xi_j)$, and owing to the independence of sink positions (at sufficiently small σ_0; see (B.7) in Appendix B for details), the covariance and variance of Q_i are given by

$$\mathbb{C}\mathrm{ov}(Q_i,Q_k) = \mathbb{V}\mathrm{ar}[Q_i] = \sum_{j=1}^{i}\mathbb{V}\mathrm{ar}[g(\xi_j)] \approx \mathrm{Pe}^2\sigma_0^2\left[1+\tfrac{3}{2}\,\mathrm{Pe}^2\sigma_0^2\right]\frac{1-\mathrm{e}^{-2\mathrm{Pe}\,i}}{\mathrm{e}^{2\mathrm{Pe}}-1}, \quad i\leqslant k. \tag{3.35}$$

Substituting (3.35), $i\sim\varepsilon^{-1}X$ and $N\sim\varepsilon^{-1}$ into (3.30) and (3.31), after some algebra, we find

$$\mathbb{V}\mathrm{ar}[C^{(1)}] \approx 2\,q_1^2\,\sigma_0^2\,(1+\tfrac{3}{2}\,\sigma_0^2\,\mathrm{Pe}^2)\,\frac{\left(\mathrm{e}^{\frac{\mathrm{Pe}}{\varepsilon}X}+\mathrm{e}^{\frac{\mathrm{Pe}}{\varepsilon}(1-X)}-\mathrm{e}^{\frac{\mathrm{Pe}}{\varepsilon}(1+X)}-\mathrm{e}^{\frac{\mathrm{Pe}}{\varepsilon}(2-X)}+\mathrm{e}^{2\frac{\mathrm{Pe}}{\varepsilon}}-1\right)}{\left(\mathrm{e}^{2\mathrm{Pe}}-1\right)(\mathrm{e}^{\frac{\mathrm{Pe}}{\varepsilon}}-1)^2}, \tag{3.36}$$

$$\begin{aligned}\mathbb{C}\mathrm{ov}_{\mathrm{T}}[C^{(1)}] \approx\; & q_1^2\,\sigma_0^2\,(1+\tfrac{3}{2}\,\sigma_0^2\,\mathrm{Pe}^2)\left(\mathrm{e}^{2\mathrm{Pe}}-1\right)^{-1}\left(\mathrm{e}^{\frac{\mathrm{Pe}}{\varepsilon}}-1\right)^{-2}\Bigg(2\mathrm{e}^{\frac{\mathrm{Pe}}{\varepsilon}X}+2\mathrm{e}^{\frac{\mathrm{Pe}}{\varepsilon}(1-X)}+\\ &+\mathrm{e}^{\frac{\mathrm{Pe}}{\varepsilon}2(1-X)}+\mathrm{e}^{\frac{\mathrm{Pe}}{\varepsilon}(1+2X)}-2\mathrm{e}^{\frac{\mathrm{Pe}}{\varepsilon}(1+X)}-2\mathrm{e}^{\frac{\mathrm{Pe}}{\varepsilon}(2-X)}-\mathrm{e}^{\frac{\mathrm{Pe}}{\varepsilon}(1-2X)}-\mathrm{e}^{\frac{\mathrm{Pe}}{\varepsilon}2X}+\mathrm{e}^{2\frac{\mathrm{Pe}}{\varepsilon}}-1\Bigg),\\ &\qquad 0\leqslant X\leqslant\tfrac{1}{2},\end{aligned} \tag{3.37}$$

where $\mathbb{C}\mathrm{ov}_{\mathrm{T}}[C^{(1)}]$ for $\frac{1}{2}<X\leqslant 1$ corresponds to substituting X with $1-X$ in (3.37), due to the symmetry of the covariance.

By taking the limit of (3.36) and (3.37) for small $\mathrm{Pe}\ll O(\varepsilon)$, we find at leading order $\mathbb{V}\mathrm{ar}[C^{(1)}]\simeq\varepsilon^{-1}q_1^2\sigma^2X(1-X)$ and $\mathbb{C}\mathrm{ov}_{\mathrm{T}}[C^{(1)}]\simeq\varepsilon^{-1}q_1^2\sigma^2X^2$, which are identical to the variance (3.13) and transverse covariance (3.14) respectively (with $q_1=\varepsilon q$).

Figure 7 shows that the theoretical predictions (3.36), (3.37) agree well with Monte-Carlo simulations at intermediate Péclet number $\mathrm{Pe}=\varepsilon^{1/2}$ ($O(\varepsilon)\ll\mathrm{Pe}\ll O(1)$), when the effect of advection on the fluctuation becomes noticeable but no boundary layer has been formed. However, (3.36) differs by a factor of ca. 1.3 for $\mathrm{Pe}=O(1)$ (Fig. 6b), which can be attributed in part to neglecting the $O(\mathrm{Pe})$ terms, compared to the leading-order $O(\mathrm{Pe}/\varepsilon)$, in the exponents of (3.36) and (3.37), and to the breakdown of the approximation (3.32) for $\mathrm{Pe}\gtrsim O(1)$. Nevertheless, (3.36) can be used to explain the boundary layer in the variance at $X=0,1$, observed in Fig. 6(b), which has width $O(\varepsilon/\mathrm{Pe})$.

In order to estimate the magnitude of the fluctuations, analogous to (3.15), we take the Chebyshev norm $\|r^\varepsilon\|_C^2\approx\max_X\mathbb{V}\mathrm{ar}[r^\varepsilon]\approx\varepsilon^2\mathbb{V}\mathrm{ar}[C^{(1)}]|_{X=1/2}$ as a conservative measure (being an upper bound of the other norms defined in (2.6)). Then (3.36) gives (after some algebra)

$$\|r^\varepsilon\|_C^2 \approx \frac{2\,\varepsilon^2\,q_1^2\,\sigma_0^2\,(1+\frac{3}{2}\,\sigma_0^2\,\mathrm{Pe}^2)}{\mathrm{e}^{2\mathrm{Pe}}-1}\,\frac{1-\mathrm{e}^{-\frac{1}{2}\frac{\mathrm{Pe}}{\varepsilon}}}{1+\mathrm{e}^{-\frac{1}{2}\frac{\mathrm{Pe}}{\varepsilon}}}, \quad q_1=\mathrm{Da}/\varepsilon. \tag{3.38}$$

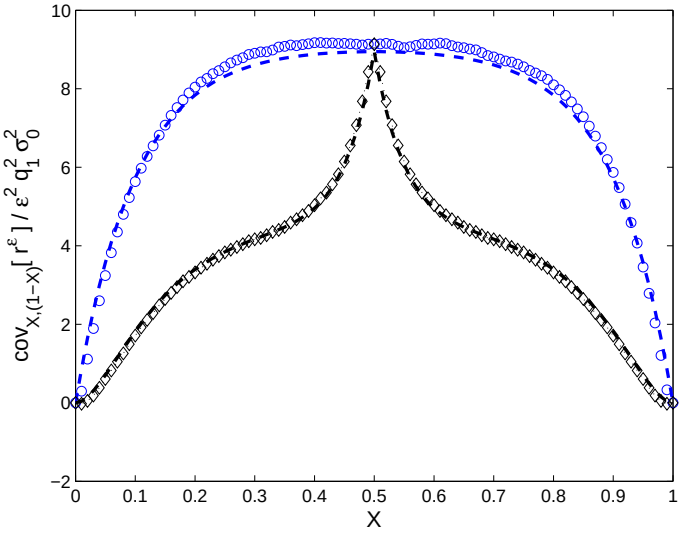

Figure 7. Monte-Carlo estimates of variance $\mathbb{V}\mathrm{ar}[r^\varepsilon]$ (blue circles) and transverse covariance $\mathbb{C}\mathrm{ov}(r^\varepsilon(X), r^\varepsilon(1-X))$ (black diamonds) for a normally-perturbed random process with $\sigma = 0.5\,\varepsilon$, computed for $\mathrm{Pe} = \varepsilon^{1/2}$, $q_1 \equiv \mathrm{Da}/(\varepsilon \mathrm{Pe}) = 1$, $\varepsilon = 0.01$, using 5×10^4 realisations; the dashed lines indicate the corresponding theoretical predictions (3.36) and (3.37). All data are scaled by $(\varepsilon\, q_1\, \sigma_0)^{-2}$.

When $\|r^\varepsilon\|_C = O(1)$, the homogenization approximation fails, defining the critical Damköhler number

$$\mathrm{Da}_{\mathrm{cr}} \approx \left\{ \frac{\mathrm{e}^{2\mathrm{Pe}} - 1}{2\,\sigma_0^2\,(1 + \frac{3}{2}\,\sigma_0^2\,\mathrm{Pe}^2)}\, \frac{1 + \mathrm{e}^{-\frac{1}{2}\frac{\mathrm{Pe}}{\varepsilon}}}{1 - \mathrm{e}^{-\frac{1}{2}\frac{\mathrm{Pe}}{\varepsilon}}} \right\}^{1/2}. \tag{3.39}$$

We can therefore divide $(\mathrm{Pe}, \mathrm{Da})$-parameter space into two regions: for $\mathrm{Pe} \lesssim O(\varepsilon)$, $\mathrm{Da}_{\mathrm{cr}} \simeq O(\sigma_0^{-1}\,\varepsilon^{1/2})$ and for $O(\varepsilon) \ll \mathrm{Pe} \ll O(1)$, $\mathrm{Da}_{\mathrm{cr}} \simeq O(\sigma_0^{-1}\,\sqrt{\mathrm{Pe}})$.

Similarly to (3.16), we also estimate under the L_2 and H^1 norms (2.6) the magnitude of the variance of the homogenization residue. Integrating (3.36) and its derivative with respect to X over $0 < X < 1$, we find (after some algebra), that

$$\varepsilon\,\|\mathbb{V}\mathrm{ar}[C^{(1)}]\|_{L_2}^{1/2} \approx \mathrm{Da}\,\sigma_0/\sqrt{\mathrm{Pe}}, \quad \varepsilon\,\|\mathbb{V}\mathrm{ar}[C^{(1)}]\|_{H^1}^{1/2} \approx \mathrm{Da}\,\sigma_0/(\varepsilon\,\mathrm{Pe})^{\frac{1}{4}} \quad \text{for} \quad \varepsilon \ll \mathrm{Pe} \ll 1,\ \sigma_0 \ll 1. \tag{3.40}$$

Comparing these to the norms for the periodic (mean) component $\|\mathbb{E}[\varepsilon C^{(1)}]\|_C = \|\mathbb{E}[\varepsilon C^{(1)}]\|_{L_2} = O(\mathrm{Da})$ and $\|\mathbb{E}[\varepsilon C^{(1)}]\|_{H^1} = O(\mathrm{Da}/\varepsilon)$ respectively (from CLDJ), we finally obtain for

$$\|r^\varepsilon\| \approx \varepsilon \left(\|\mathbb{E}[C^{(1)}]\| + \|\mathbb{V}\mathrm{ar}[C^{(1)}]\|^{1/2} \right) \tag{3.41}$$

	$\mathscr{U}(0,1)$	$\mathscr{N}(i,\sigma_0^2)$	Periodic (mean)
$\|r^\varepsilon\|_{L_2}$	$O(q\sqrt{\varepsilon})$	$O(q\sigma_0\varepsilon^{3/2})$	$O(q\varepsilon^2)$
$\|r^\varepsilon\|_{H^1}$	$O(q\sqrt{\varepsilon})$	$O(q\varepsilon)$	$O(q\varepsilon)$

Table 1. Asymptotic convergence rates of the homogenization residue, for a periodic array (CLDJ) and random arrays (based on the analytical results of § 3.2) in the mean-squared (L_2) and Sobolev (mean-squared with the first derivative; H^1) norms at $\mathrm{Pe} \lesssim \varepsilon$ ($q = \mathrm{Da}/\varepsilon^2$, $\sigma_0 = \sigma/\varepsilon \lesssim 1$).

the estimates

$$\|r^\varepsilon\|_C \simeq \|r^\varepsilon\|_{L_2} \simeq O(\mathrm{Da}\,\sigma_0/\sqrt{\mathrm{Pe}}), \quad \|r^\varepsilon\|_{H^1} \simeq O(\mathrm{Da}/\varepsilon) \quad \text{for} \quad \varepsilon \ll \mathrm{Pe} \ll 1,\ \sqrt{\mathrm{Pe}} < \sigma_0 \ll 1. \tag{3.42}$$

We now combine the results to survey the accuracy of the homogenization approximation in (Pe, Da)-parameter space for different stochastic sink distributions.

4. Applicability and accuracy of the homogenization approximation on random arrays

Based on the analytical and numerical results of § 3.1, 3.2 and 3.3 we can estimate the error bounds of the solute transport homogenization (the magnitude of the residue r^ε), using (3.15) for "strong" (H^1) and "weak" (L_2) norms (2.6). The regions of H^1 (L_2)-convergence in (Pe, Da)-space are defined as $\|r^\varepsilon\|_{H^1} \lesssim O(1)$ ($\|r^\varepsilon\|_{L_2} \lesssim O(1)$). Table 1 summarises our findings for f_n (3.16) and f_u (3.20) at $\mathrm{Pe} \lesssim \varepsilon$ (results for the periodic case are from CLDJ). When diffusion dominates at the microscale ($\mathrm{Pe} = O(\varepsilon)$, $\mathrm{Da} = O(\varepsilon^2)$), the magnitude of the pointwise variance depends strongly on the degree of periodicity in the underlying structure, with fluctuations rising from $O(q\varepsilon^{3/2})$ for almost periodic sink distributions to $O(q\varepsilon^{1/2})$ for uniformly random sink distributions. The corresponding regions of convergence for $\mathrm{Pe} \lesssim \varepsilon$ with a uniformly-random (f_u) sink distribution are illustrated in Figure 8(a); the corresponding map for a normally-perturbed periodic array (f_n) is shown in Figure 8(b). The weak and strong convergence boundaries at $\mathrm{Da} = O(1)$ and $\mathrm{Da} = O(\varepsilon)$ in the periodic case shrink to $\mathrm{Da} = O(\varepsilon^{1/2})$ and $\mathrm{Da} = O(\varepsilon)$ with $f = f_n$ and to $\mathrm{Da} = O(\varepsilon^{3/2})$ with $f = f_u$. In addition, we employ (3.42) to assess the accuracy of the homogenization approximation for f_n-distributed sinks in the intermediate range of Péclet number ($\varepsilon \ll \mathrm{Pe} \ll 1$). Now the weak convergence boundary $\mathrm{Da} = O(1)$ for $\varepsilon \ll \mathrm{Pe} \ll 1$ for periodic sinks is replaced by $\mathrm{Da} = O(\sqrt{\mathrm{Pe}})$ when $f = f_n$; the strong convergence boundary at $\mathrm{Da} = O(\varepsilon)$ is unaltered.

Motivated by the accuracy of periodic homogenization from CLDJ (thick dashed lines and dash-dotted lines in Fig. 8(a,b)) and informed by the analytical magnitudes of fluctuations in the homogenization residue and its gradient at $\mathrm{Pe} \lesssim \varepsilon$ (Table 1), we conjecture the convergence regions for f_u and f_n at $\mathrm{Pe} \gtrsim 1$, based on Monte-Carlo simulations. Figure 8(c,d) show convergence results determined by Monte-Carlo simulations when $(\mathrm{Pe}, \mathrm{Da}) = (1, \varepsilon^2)$ (point (1) in Fig. 8a) and $(\mathrm{Pe}, \mathrm{Da}) = (\varepsilon^{-1/2}, \varepsilon^{3/2})$ (point (2)) with f_u-distributed sinks. Panel (c) in Figure 8 shows $\|r^\varepsilon\|_{L_2} \sim \varepsilon^{3/2}$ in a manner independent of Pe, Da for points (1) and (2). Assuming that $\|r^\varepsilon\|_{L_2}$ is linear in Da (due to linearity of the original problem (2.1)), so that $\|r^\varepsilon\|_{L_2} \sim \mathrm{Da}\,\varepsilon^\beta\,\mathrm{Pe}^\gamma$ and $\|r^\varepsilon\|_{L_2} \sim \varepsilon^{3/2}$ at each point tested, it follows that $\|r^\varepsilon\|_{L_2} \sim \mathrm{Da}/(\sqrt{\varepsilon}\,\mathrm{Pe})$ for $\mathrm{Pe} \gtrsim 1$, which lies below the periodic-sink-distribution threshold Da/Pe. Likewise, assuming $\|r^\varepsilon\|_{H^1} \sim \mathrm{Da}\,\varepsilon^{\beta_1}\,\mathrm{Pe}^{\gamma_1}$,

it follows from the scaling illustrated in Fig. 8(d) that $\|r^\varepsilon\|_{H^1} \sim \mathrm{Da}/(\varepsilon\sqrt{\mathrm{Pe}})$ for $\mathrm{Pe} \gtrsim 1$ (as in the periodic case). While not a formal proof of convergence, these conjectured boundaries are extrapolated into $\mathrm{Pe} > 1$ in Fig. 8(a), while those arising from Table 1 and (3.42) are plotted for $\mathrm{Pe} \lesssim 1$. Analogous Monte-Carlo simulations for the f_n-distribution with $\sigma_0 = 0.5$ (not shown) agree with the conjectured boundaries $\|r^\varepsilon\|_{L_2} \sim \mathrm{Da}/\mathrm{Pe}$ and $\|r^\varepsilon\|_{H^1} \sim \mathrm{Da}/(\varepsilon\sqrt{\mathrm{Pe}})$ for $\mathrm{Pe} \gtrsim 1$, plotted in Fig. 8(b), both of which match the periodic-sink case.

Thus, the effect of stochasticity on the convergence rates is greatest for small Péclet number $\mathrm{Pe} \ll 1$, while the presence of strong advection seems to make the homogenization approximation less sensitive to the fluctuations due to the irregular microstructure. Interestingly, in the case of a uniformly random distribution (Fig. 8a) for $\mathrm{Pe} \ll \varepsilon$, the magnitude of the fluctuations is such that the region of strong convergence in $\|\cdot\|_{H^1}$ (medium shade/green) and the region of divergence (dark shade/red) of the homogenization residue collapse to eliminate the transitional weak convergence region in $\|\cdot\|_{L_2}$ (light shade/yellow). In the region of divergence of stochastic homogenization (dark shade/red in Fig. 8(a,b), below the thick dashed lines) the "noise-to-signal" ratio becomes larger than 1, and thus a particular realisation of the random array cannot be neglected in calculating the macroscopic transport. The normally-perturbed distribution f_n with small standard deviation $\sigma \equiv \varepsilon\sigma_0$ therefore takes a distinct position among the considered random geometries, in terms of preserving high homogenization accuracy, particularly at small Pe.

5. Discussion

In the present paper we have analysed the spatial correlation and magnitude of fluctuations (about the leading-order homogenization approximation) of a scalar quantity transported by advection and diffusion past an irregular array of sinks. We have shown in particular how fluctuations can be expressed as a functional of the sink locations. At low Pe, this functional is linear. In CLDJ, we derived resulting expressions for the distribution over the domain of the pointwise variance of fluctuations; here we have derived the corresponding pointwise covariance of fluctuations for uniformly random and normally perturbed sink distributions (3.14, 3.19). These results reveal the multiscale structure of the homogenization residue: fluctuations appear to be correlated over lengthscales comparable to the whole domain (Fig. 5) even when sink distributions are correlated only over short distances. When $\mathrm{Pe} = O(1)$, the functional connecting fluctuations to sink locations becomes nonlinear and evaluating the statistical properties of the fluctuations is less straightforward. To analyse this case, we used an approximation that is sufficient to capture the structure of the variance and covariance for normally perturbed sinks for small but finite Pe ((3.36–3.37), Figs 6(b), 7); extending these results to larger Pe and to uniformly random sink distributions remains an interesting open problem. Curiously, advection changes the shape of the fluctuation distribution without inducing an asymmetry in the flow direction, at least for the examples examined here (Figs 3(c,d), 6(b), 7), emphasising the equal importance of the global inlet and outlet boundary conditions.

These results, combined with direct Monte-Carlo simulations, were then used to characterise the convergence of the homogenization approximation across $(\mathrm{Pe}, \mathrm{Da})$-parameter space for different sink distributions. The magnitude of the homogenization residue falls for distributions with a greater degree of periodicity but grows with increasing sink strength (CLDJ). In Fig. 3(a) of CLDJ we identified the domains of convergence (under two representative norms) of the homogenization approximation for a periodic sink distribution. Figure 8(a,b) extends these results to uniformly random and normally perturbed sink distributions respectively. There is a pronounced shrinkage of the domain of convergence, especially for small Péclet number (Table 1), which increases with the loss of regularity in the sink distributions, in a manner illustrated clearly for individual realisations in Figs 4(a) and 4(b). Thus corrections to the leading-order approximation can be significant even when the exact solution is sufficiently smooth. The character of the fluctuations

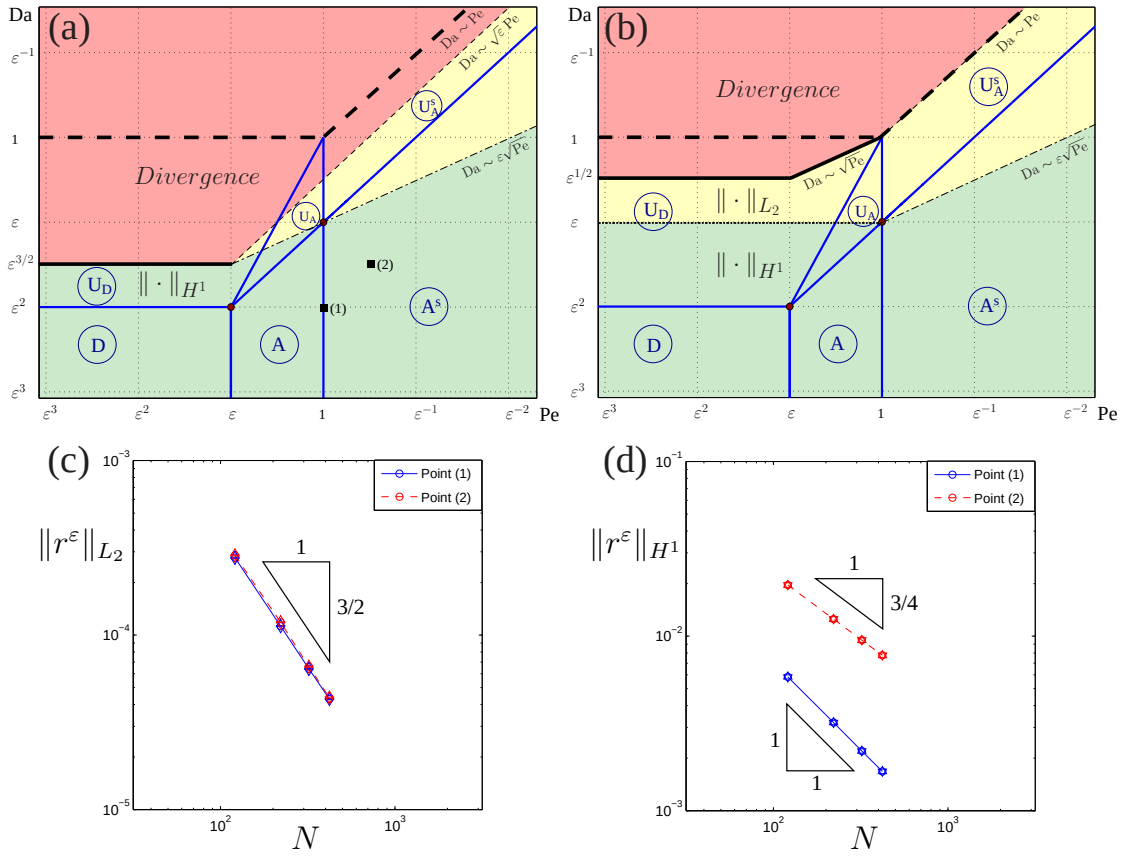

Figure 8. (a,b) Types of convergence in (Pe, Da)-space for stochastic homogenization of solute transport at small-to-moderate Pe with (a) uniformly random distributed sinks, and (b) normally-perturbed sinks (for $\sigma_0 = O(1)$). Grey/blue thin solid lines bound the asymptotic regimes (D, A, $\mathrm{U_D}$, $\mathrm{U_A}$, $\mathrm{U_A^s}$, $\mathrm{A^s}$) illustrated in Fig. 1. The region of "strong" convergence in the Sobolev (H^1) norm is shown in medium shade/green, the region of "weak" convergence in the mean-squared (L_2) norm is in light shade/yellow, and the region of global divergence (in L_2-norm) is in dark shade/red (plotted for $\varepsilon = 0.05$). Solid boundaries in $\mathrm{Pe} \lesssim 1$ are as identified in Table 1 and (3.42). The black thick dashed lines in (a,b) indicate the border of the divergence region in the case of a periodic array (CLDJ); thin dashed and dash-dotted lines conjecture, based on Monte-Carlo simulations, the upper boundaries of L_2 and H^1-convergence respectively for higher Pe. (c,d) Monte-Carlo simulation of convergence rates for the points (1) $\mathrm{Pe} = 1$, $\mathrm{Da} = \varepsilon^2$ (solid line) and (2) $\mathrm{Pe} = \varepsilon^{-1/2}$, $\mathrm{Da} = \varepsilon^{3/2}$ (dashed line) from the parameter space (a) (ensemble average over 1000 samples for each $N \sim \varepsilon^{-1}$); triangles indicate a slope in accord to the scaling of the thin dashed ($\mathrm{Da} \sim \sqrt{\varepsilon}\,\mathrm{Pe}$) and dash-dotted ($\mathrm{Da} \sim \varepsilon\sqrt{\mathrm{Pe}}$) lines in (a) (with both points lie parallel to the former but not to the later lines).

at low Pe is sensitive to the sink distribution, with sharper gradients arising between normally perturbed sinks than between uniformly random sinks (compare Figs 4(c) and 4(d)). This reflects the fact that the breakdown of the homogenization approximation in the uniformly random case for $\mathrm{Pe} \ll \varepsilon$ bypasses the regime of weak convergence (Fig. 8a): fluctuations are relatively smooth but grow rapidly in magnitude as Da increases. At higher Pe (Fig. 3), for both sink distributions that we examined, convergence is influenced both by the magnitude of fluctuations and large inter-sink gradients, allowing regimes of weak and strong convergence to be identified. An important factor contributing to the deviation of the exact solution from the homogenization approximation is the clustering of sinks that is evident in Fig. 3(a,b). This might be analysed in future studies by considering arrays of sinks of varying strength with larger inter-sink distance, or by introducing a lengthscale for inter-cluster spacing ε_1 that is intermediate between the microscale ε and the global scale 1 ($\varepsilon \ll \varepsilon_1 \ll 1$), and then performing reiterated homogenization Bensoussan *et al.* (1978).

We can compare our analytical and numerical predictions with existing theoretical results for random homogenization of problems similar to (2.1) that take into account the spatial autocorrelation properties of the coefficients of corresponding governing equations. Bourgeat & Piatnitski (1999) show in their Lemma 4.2 that the homogenization error of a one-dimensional diffusion-reaction equation ($\mathrm{Pe} = 0$) is $\mathbb{E}[\max_X |r^\varepsilon(X)|^2]^{1/2} \leqslant O(\sqrt{\varepsilon})$ when the diffusion coefficient is a stationary random process with "short-term memory", and $\mathbb{E}[\max_X |r^\varepsilon|^2]^{1/2} \leqslant O(\varepsilon^{\gamma/2})$ for a "long-term memory" coefficient ($0 < \gamma < 1$). Bal & Jing (2010) generalise these results for a linear transport-attenuation-scattering equation in two and three dimensions and show that, when the equation coefficients are bounded functions of a Poisson point process (with short-term memory, $\gamma > 1$), the following estimate holds: $\mathbb{E}[\,\|r^\varepsilon\|_{L_2}^2\,]^{1/2} \leqslant O(\sqrt{\varepsilon})$. Since the source term in (2.1), defined by a sink distribution, is a short-term-memory stationary process, one might expect a similar upper bound on the residue r^ε being applicable. We indeed observe that the homogenization error for both stochastic sink distributions considered here are bounded by $O(\sqrt{\varepsilon})$ for $\mathrm{Pe} \gtrsim 1$, when $\mathrm{Da} = O(\varepsilon \mathrm{Pe})$ (data not shown; see also Chernyavsky (2011)). This upper bound is exact for a uniformly-random distributions; however, it considerably overestimates the error in the case of a normally-perturbed sink distribution (which can be as low as $O(\varepsilon)$ for this parameter regime), highlighting the importance of distribution-specific error estimation.

The present problem was chosen to be deliberately simple in order to allow analytical progress. Many extensions might be usefully explored. In CLDJ, for example, we reported results for sinks satisfying a hard-core distribution (for which sinks are distributed sequentially from a uniform distribution provided they do not fall within a prescribed distance d of an existing sink). The statistics of fluctuations resemble those of a uniformly random distribution (Fig. 4(d,e) of CLDJ) when d is sufficiently small (just as fluctuations over an array of normally perturbed sinks become essentially indistinguishable from those over a uniformly random array when $\sigma \gtrsim 0.3$). Even though the hard-core process appears empirically closer to a periodic array for larger d, the solution over a hard-core array converges slower to $C^{(0)}$ than that over a normally-perturbed array for sufficiently small ε (data not shown), because of the lower degree of long-range correlation in sink locations for normally perturbed sinks.

Another obvious extension of the present model is to consider other types of uptake kinetics. We demonstrate in Appendix A that moving from zeroth to higher-order kinetics retains the gross features of the leading-order analysis, with the leading-order homogenization approximation satisfying $C^{(0)}_{XX} - pC^{(0)}_X = q\left(C^{(0)}\right)^\alpha$. The corrections to $C^{(0)}$ obtained on a periodic array in CLDJ for $\alpha = 0$ also remain valid for $\alpha > 0$, substituting q with $q\,(C^{(0)}(X))^\alpha$, i.e. the bounds on the homogenization residue become spatially non-uniform, varying slowly over the array. However, a more detailed analysis of fluctuations for $\alpha > 0$ remains the subject of future work.

Finally, it is of interest to consider further extensions of the present approach to problems in two or three dimensions and to sinks of finite size, so that the accuracy of homogenization approximations for flow and transport problems in random porous media (of the variety illustrated in Figure 1) can be assessed for different classes of stochastic geometries.

A. Transport with power-law uptake kinetics on a periodic array

We consider a model generalising (2.1) that is given by

$$\frac{\mathrm{d}^2C}{\mathrm{d}x^2} - \mathrm{Pe}\frac{\mathrm{d}C}{\mathrm{d}x} = \mathrm{Da}\, f(x) C^{\alpha}, \quad f = \sum_{i=1}^{N} \delta(x-\xi_i), \quad 0 < x < \varepsilon^{-1}, \tag{A.1a}$$

$$C|_{x=0} = 1, \quad C|_{x=\varepsilon^{-1}} = 0 \ \text{ or } \ C|_{x=x_0} = \left.\frac{\mathrm{d}C}{\mathrm{d}x}\right|_{x=x_0} = 0, \tag{A.1b}$$

where $\mathrm{Pe} = u_0 l/D$ is the microscopic Péclet number, and $\mathrm{Da} = q_0 l/(DC_0^{1-\alpha})$ is the microscopic Damköhler number and α is the order of uptake kinetics (thus q_0 is measured in $\mathrm{mol}\cdot\mathrm{s}^{-1}\cdot\mathrm{m}^{-2}$ for zero-order uptake ($\alpha = 0$) and in $\mathrm{m}\cdot\mathrm{s}^{-1}$ for first-order uptake ($\alpha = 1$)).

We look for an approximate x-periodic solution to (2.1) about the organising centre $\mathrm{Pe} = \varepsilon p$, $\mathrm{Da} = \varepsilon^2 q$ ($p, q = O(1)$) in the form of a two-scale asymptotic power series (2.2). Substituting (2.2) and (2.3) into (A.1) and collecting terms in powers of ε, we get at $O(1)$

$$C^{(0)} = C^{(0)}(X); \quad C^{(0)}|_{X=0} = 1, \quad C^{(0)}|_{X=1} = 0 \ \text{ or } \ C^{(0)}|_{X=X_0} = C^{(0)}_X|_{X=X_0} = 0. \tag{A.2}$$

At $O(\varepsilon)$, we find that $C^{(1)} \equiv 0$, and at $O(\varepsilon^2)$, we obtain

$$C^{(0)}_{XX} - pC^{(0)}_X = -C^{(2)}_{xx} + q\big(C^{(0)}\big)^{\alpha} \sum_{i=1}^{N} \delta(x-i) \tag{A.3a}$$

$$C^{(2)} \ \text{ is } x\text{-periodic}. \tag{A.3b}$$

Integrating (A.3a) over a unit cell $-1/2 \leqslant x - i \leqslant 1/2$, we finally have

$$C^{(0)}_{XX} - pC^{(0)}_X = q\left(C^{(0)}\right)^{\alpha}, \tag{A.4}$$

subject to the global boundary conditions. Solution and detailed analysis for $\alpha = 0$ is given in CLDJ. For first-order kinetics ($\alpha = 1$), equation (A.4) has the solution

$$C^{(0)} = \mathrm{e}^{pX/2} \sinh\left(\sqrt{q + p^2/4}(1-X)\right) / \sinh\sqrt{q + p^2/4}, \tag{A.5}$$

shown in Figure A.1. At large Pe, neglecting the diffusive boundary layer at the outlet, this simplifies to $C^{(0)} = \mathrm{e}^{-(q/p)X}$ (*cf.* $C^{(0)} = 1 - (q/p)X$ for zeroth-order uptake; see also the general expression (2.4)). Both global advective and uptake fluxes are approximately balanced when $q \sim p \gg 1$ (as showed by the asymptotic line $\mathrm{Da} = \varepsilon\mathrm{Pe}$ in Fig. 1); however this balance is more sensitive to the change in Da/Pe ra-

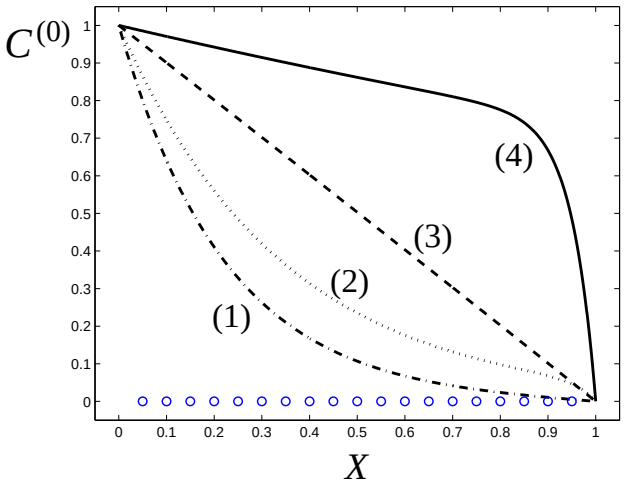

Figure A.1. Leading-order approximation $C^{(0)}$ for transport with first-order uptake ($\alpha = 1$) past a periodic sink distribution. Concentration profiles (A.5) for points (1-4) in the $(\mathrm{Pe}, \mathrm{Da})$-parameter space ($\mathrm{Pe} = \varepsilon^2, 1, \varepsilon^2, 1$ and $\mathrm{Da} = \varepsilon, \varepsilon^{0.6}, \varepsilon^3, \varepsilon^{1.4}$), corresponding to the transport regimes $\mathrm{U_D}$, $\mathrm{U_A}$, D, A defined in Fig. 1 (computed for $\varepsilon = 0.05$; circles show the locations of the 19 sinks).

tio in the case of $\alpha = 1$ than for $\alpha = 0$, owing to the exponential rather than linear decay in the solute concentration.

Substituting (A.4) into (A.3) and using the global boundary condition $C^{(2)}|_{X=0} = 0$, we find the first non-vanishing correction to $C^{(0)}$ in a unit cell: $C^{(2)} = -\frac{q}{2}(C^{(0)})^{\alpha}(x^2 - |x|)$, which becomes of the same order of magnitude as $C^{(1)}$ for $q = O(\varepsilon^{-1})$ ($\mathrm{Da} = O(\varepsilon)$), suggesting the second organising centre at $\mathrm{Da} = O(\varepsilon)$, $\mathrm{Pe} = O(1)$.

Analogously, substituting (2.2) and (2.3) into (A.1) around the second organising centre $\mathrm{Pe} = O(1)$, $\mathrm{Da} = O(\varepsilon) = \varepsilon q_1$, and collecting terms in powers of ε, we get the following problem for the correction to $C^{(0)}$ in a single unit cell $-1/2 \leqslant x' = x - i \leqslant 1/2$ (prime over x is omitted):

$$C^{(1)}_{xx} - \mathrm{Pe}\, C^{(1)}_x = \mathrm{Pe}\, C^{(0)}_X + q_1 \left(C^{(0)}\right)^{\alpha} \delta(x), \qquad C^{(1)} \ \text{ is } x\text{-periodic}, \tag{A.6a}$$

which has a solution

$$C^{(1)}(x) = \frac{q_1 \left(C^{(0)}\right)^{\alpha}}{\mathrm{Pe}} \left(-\frac{\exp\left(\mathrm{Pe}\left(x \pm \frac{1}{2}\right)\right)}{2\sinh(\mathrm{Pe}/2)} + x + \frac{\coth(\mathrm{Pe}/2) \pm 1}{2} \right), \tag{A.7}$$

for $0 < \mp x \leqslant 1/2$, where the global boundary condition (A.1b) is used to derive the local condition $C^{(1)}(0) = 0$. Comparing (A.7) to the correction obtained in Eqn. (A12) of CLDJ for $\alpha = 0$, we note that the uniform ratio q_1/Pe is replaced with a slowly varying correction magnitude $q_1 (C^{(0)})^{\alpha}/\mathrm{Pe}$ in the case $\alpha > 0$. Therefore, the upper limit on the applicability of homogenization is changed from $\mathrm{Da} \ll \max\{1, \mathrm{Pe}\}$ to $\mathrm{Da}\left(C^{(0)}\right)^{\alpha} \ll \max\{1, \mathrm{Pe}\}$, thus becoming heterogeneous over the array. Otherwise, the leading-order

regimes depicted in Figure 1 remain valid for $\alpha \geqslant 0$.

B. Moments of a sink statistics functional

In this Appendix we derive the mean and transverse covariance of the linear (3.6) and nonlinear (3.26) partial sums of the sink statistics needed to compute the correlation properties of the homogenization residue in § 3.2 and 3.3.

B.1. *Normally-perturbed periodic array (f_n)*

We first consider a normally-perturbed periodic array $\xi_j \sim \mathscr{N}(j, \sigma_0^2) \sim j + \sigma_0 \mathscr{N}(0,1)$, i.e. $\mathbb{E}[\xi_j] \equiv \mu_j = j$ and $\mathbb{V}\mathrm{ar}[\xi_j] = \sigma_0^2$ ($\sigma \equiv \sigma_0 \varepsilon$, taking $\sigma_0 \ll 1$ in order for sinks not to swap places) and compute the moments of (3.6)

$$R_i = \sum_{j=1}^{i} \xi_j \,, \quad i = 1, \ldots, N \,.$$

Owing to the independence of ξ_i for small σ_0, using the linearity property of expectation $\mathbb{E}\left[\sum_{j=1}^{i} \xi_j\right] = \sum_{j=1}^{i} \mu_j = i(i+1)/2$ and the property of a non-central χ^2 distribution with one degree of freedom $\mathbb{E}[\xi_j^2] = \mu_j^2 + \sigma_0^2$, $\mu_j \equiv j$, we have

$$R_i \sim \sum_{j=1}^{i} \mathscr{N}(j, \sigma_0^2) \sim \mathscr{N}\left(\tfrac{i(i+1)}{2}, i\sigma_0^2\right) . \tag{B.1}$$

It remains to obtain $\mathbb{C}\mathrm{ov}(R_k, R_p) \equiv \mathbb{E}[R_k R_p] - \mathbb{E}[R_k]\,\mathbb{E}[R_p]$ for $k \neq p$. The independence of ξ_j and ξ_l, i.e. $\mathbb{C}\mathrm{ov}(\xi_j, \xi_l) = 0$, for $j \neq l$, assuming that σ_0 is small enough for sinks not to swap places and $k \leqslant p$, gives

$$\begin{aligned} \mathbb{C}\mathrm{ov}(R_k, R_p) = \sum_{j=1}^{k}\sum_{l=1}^{p} \{\mathbb{E}[\xi_j \xi_l] - \mathbb{E}[\xi_j]\,\mathbb{E}[\xi_l]\} = \sum_{j=1}^{k}\sum_{l=1}^{k} \{\mathbb{E}[\xi_j \xi_l] - \mathbb{E}[\xi_j]\,\mathbb{E}[\xi_l]\} + \\ + \sum_{j=1}^{k}\sum_{\substack{l=k+1 \\ (l\neq j)}}^{p} \mathbb{C}\mathrm{ov}(\xi_j, \xi_l) = \mathbb{E}\left[\sum_{j=1}^{k}\sum_{l=1}^{k} \xi_j \xi_l\right] - \mathbb{E}\left[\sum_{j=1}^{k} \xi_j\right] \mathbb{E}\left[\sum_{l=1}^{k} \xi_l\right] = \mathbb{V}\mathrm{ar}[R_k] \,, \end{aligned} \tag{B.2}$$

reducing the covariance (for $k \leqslant p$) to the corresponding variance.

We now turn to the case of the nonlinear functional of sink distribution Q_i given by (3.26)

$$Q_i = \sum_{j=1}^{i} \mathrm{e}^{-Pe\,\xi_j} \,, \quad \xi_i \sim \mathscr{N}(i, \sigma_0^2), \quad i = 1, \ldots, N \,,$$

were $\mathbb{E}[\xi_i] \equiv \mu_i = i$, $\mathbb{V}\mathrm{ar}[\xi_i] = \sigma_0^2$.

Assuming small standard deviation $\sigma_0/\mu_i \ll 1$, we can find the corresponding expectation, variance and covariance for $g(\xi_i) = \mathrm{e}^{-\mathrm{Pe}\,\xi_i}$ by assuming g has an approximately normal distribution, and expanding it

about the mean μ_i:

$$\mathbb{E}[g(\mu_i+(\xi_i-\mu_i))]\approx g_i+\tfrac{1}{2}g_i''\,\mathbb{V}\mathrm{ar}[\xi_i]+\tfrac{1}{24}g_i''''\,\mathbb{E}[(\xi_i-\mu_i)^4]+\dots,\quad g_i\equiv g(\mu_i)\,. \tag{B.3}$$

For a normally distributed ξ_i with $\mathbb{E}[(\xi_i-\mu_i)^4]=3\,\sigma_0^4$, (B.3) gives

$$\mathbb{E}[Q_i]\equiv\sum_{j=1}^{i}\mathbb{E}[g(\xi_j)]\approx\left[1+\tfrac{1}{2}\,\mathrm{Pe}^2\sigma_0^2+\tfrac{1}{8}\,\mathrm{Pe}^4\sigma_0^4\right]\sum_{j=1}^{i}\mathrm{e}^{-\mathrm{Pe}\,j}=\left[1+\frac{\mathrm{Pe}^2\sigma_0^2}{2}+\frac{\mathrm{Pe}^4\sigma_0^4}{8}\right]\frac{1-\mathrm{e}^{-\mathrm{Pe}\,i}}{\mathrm{e}^{\mathrm{Pe}}-1}\,, \tag{B.4}$$

where we used the geometric progression $\sum_{j=1}^{n}s^j=s(s^n-1)/(s-1)$ to compute the sum.

Analogously

$$\mathbb{V}\mathrm{ar}[g(\xi_i)]\equiv\mathbb{E}[g(\xi_i)^2]-(\mathbb{E}[g(\xi_i)])^2\approx(g_i')^2\,\mathbb{V}\mathrm{ar}[\xi_i]+\left(\tfrac{1}{3}\,g_i'g_i'''+\tfrac{1}{6}\,(g_i'')^2\right)\mathbb{E}[(\xi_i-\mu_i)^4]\,, \tag{B.5}$$

and since $\mathbb{V}\mathrm{ar}[Q_i]=\sum_{j=1}^{i}\sum_{k=1}^{i}\{\mathbb{E}[g(\xi_j)g(\xi_k)]-\mathbb{E}[g(\xi_j)]\,\mathbb{E}[g(\xi_k)]\}=\sum_{j=1}^{i}\mathbb{V}\mathrm{ar}[g(\xi_j)]$ due to the independence of ξ_j and ξ_k, i.e. $\mathbb{C}\mathrm{ov}(g(\xi_i),g(\xi_k))=0$, for $j\neq k$ and small σ_0, we get from (B.5) the variance

$$\mathbb{V}\mathrm{ar}[Q_i]\approx\mathrm{Pe}^2\sigma_0^2\left[1+\tfrac{3}{2}\,\mathrm{Pe}^2\sigma_0^2\right]\sum_{j=1}^{i}\mathrm{e}^{-2Pe\,j}=\mathrm{Pe}^2\sigma_0^2\left[1+\tfrac{3}{2}\,\mathrm{Pe}^2\sigma_0^2+O(\sigma_0^4)\right]\frac{1-\mathrm{e}^{-2\mathrm{Pe}\,i}}{\mathrm{e}^{2\mathrm{Pe}}-1}\,. \tag{B.6}$$

It remains to find the covariance $\mathbb{C}\mathrm{ov}(Q_i,Q_k)=\mathbb{E}[Q_iQ_k]-\mathbb{E}[Q_i]\,\mathbb{E}[Q_k]$ for $i\neq k$. We denote $\mathring{g}_i\equiv g(\xi_i)-\mathbb{E}[g(\xi_i)]$, so that $\mathbb{E}[\mathring{g}_i]=0$ and $\mathbb{E}[\mathring{g}_i^2]=\mathbb{V}\mathrm{ar}[g(\xi_i)]$. Then, for $i\leqslant k$,

$$\begin{aligned}\mathbb{C}\mathrm{ov}(Q_i,Q_k)&=\sum_{j=1}^{i}\sum_{l=1}^{k}\mathbb{E}[\mathring{g}_j\mathring{g}_l]=\sum_{j=1}^{i}\mathbb{E}[\mathring{g}_j^2]+\sum_{j=1}^{i}\sum_{\substack{l=1\\(l\neq j)}}^{k}\mathbb{E}[\mathring{g}_j\mathring{g}_l]\\&=\sum_{j=1}^{i}\mathbb{V}\mathrm{ar}[g(\xi_j)]+\sum_{j=1}^{i}\sum_{\substack{l=1\\(l\neq j)}}^{k}\mathbb{C}\mathrm{ov}(g(\xi_i),g(\xi_k))\,,\end{aligned} \tag{B.7}$$

with the first sum on the right-hand side of (B.7) being equal to (B.6) and the second sum vanishing due to the independence of $g(\xi_j)$ and $g(\xi_l)$, i.e. $\mathbb{C}\mathrm{ov}(g(\xi_i),g(\xi_k))=0$ $(j\neq l)$, for sufficiently small σ_0, providing the covariance

$$\mathbb{C}\mathrm{ov}(Q_i,Q_k)=\mathbb{V}\mathrm{ar}[Q_i]\,,\quad i\leqslant k\,, \tag{B.8}$$

which is given by (B.6).

By repeating the calculations (B.3)–(B.6) up to $O(\sigma_0^6)$, taking into account that $1/\sqrt{2\pi}\int_{-\infty}^{\infty}t^6\,\mathrm{e}^{-t^2/2}dt=15$ and hence $\mathbb{E}[(\xi_i-\mu_i)^6]=15\,\sigma_0^6$, we find, after some algebra, that $\mathbb{V}\mathrm{ar}[Q_i]\sim\mathrm{Pe}^2\sigma_0^2\,[1+\frac{3}{2}\,\mathrm{Pe}^2\sigma_0^2+\frac{7}{6}\,\mathrm{Pe}^4\sigma_0^4+O(\sigma_0^6)]\simeq\mathrm{e}^{\mathrm{Pe}^2\sigma_0^2}(\mathrm{e}^{\mathrm{Pe}^2\sigma_0^2}-1)$, which is related to the variance of the log-normal distribution of $\mathrm{e}^{-\mathrm{Pe}\,\xi_i}$ (Korn & Korn, 2000).

B.2. *Uniformly random array (f_u)*

When $f = f_u$, we turn to Matsunawa (1985), who determined the distribution of linear combinations of order statistics drawn from $\mathscr{U}(0,1)$ (i.e. combinations of $\hat{\xi}_1,\ldots,\hat{\xi}_N$, where $\hat{\xi}_i \equiv \varepsilon\xi_i$) as a mixture of scaled Beta distributions.

Let us consider $\hat{\xi}_i$, $i = 1,\ldots,N$ to be the ordered values from a sample of N independent uniformly distributed random variables on $[0,1]$, where $\hat{\xi}_i < \hat{\xi}_j$ for $i < j$, and also set $\hat{\xi}_0 = 0$ and $\hat{\xi}_{N+1} = 1$ to account for the boundary conditions. Let $V_i = \hat{\xi}_i - \hat{\xi}_{i-1}$, $i = 1,\ldots,N+1$ and so $(V_1,\ldots,V_{N+1})$ has a Dirichlet distribution with $(N+1)$-vector of parameters $(1,1,\ldots,1)$ Matsunawa (1985). From the properties of the Dirichlet distribution we know that

$$\mathbb{E}[V_i] = \frac{1}{N+1}, \quad \mathbb{V}\mathrm{ar}[V_i] = \frac{N}{(N+1)^2(N+2)}, \quad \mathbb{C}\mathrm{ov}(V_i,V_j) = \frac{-1}{(N+1)^2(N+2)}, \tag{B.9}$$

where $i \neq j$, $i,j = 1,\ldots,N$.

Consider the partial sums of order statistics $\hat{\xi}_i$

$$L_k = \sum_{j=1}^{k} b_j V_j, \quad T_p = \sum_{q=1}^{p} c_q V_q, \tag{B.10}$$

where b_j, c_q are given deterministic weights. Then, from (B.9) and the linearity property of expectation we have

$$\mathbb{E}[L_k] = \sum_{j=1}^{k} b_j \mathbb{E}[V_j] = \frac{\sum_{j=1}^{k} b_j}{N+1}, \tag{B.11a}$$

$$\mathbb{V}\mathrm{ar}[L_k] = \sum_{j=1}^{k}\sum_{l=1}^{k} b_j b_l \mathbb{C}\mathrm{ov}(V_j,V_l) = \frac{\sum_{j=1}^{k} b_j^2}{(N+1)(N+2)} - \frac{\sum_{j=1}^{k}\sum_{l=1}^{k} b_j b_l}{(N+1)^2(N+2)}, \tag{B.11b}$$

$$\mathbb{C}\mathrm{ov}(L_k,T_p) = \sum_{j=1}^{k}\sum_{q=1}^{p} b_j c_q \mathbb{C}\mathrm{ov}(V_j,V_q) = \frac{\sum_{j=1}^{k}\sum_{q=1}^{p} b_j c_q \left\{(N+1)\delta_{jq} - 1\right\}}{(N+1)^2(N+2)}, \tag{B.11c}$$

where $k,p = 1,\ldots,N$, $k \leqslant p$ and δ_{jq} is the Kronecker delta-function.

We now consider expressions for the mean, variance and covariance of the partial sums R_k of the order statistics:

$$R_k \equiv \varepsilon^{-1}\sum_{j=1}^{k}\hat{\xi}_j \equiv \sum_{j=1}^{k}(k-j+1)V_j, \quad R_p \equiv \varepsilon^{-1}\sum_{q=1}^{p}\hat{\xi}_q \equiv \sum_{q=1}^{p}(p-q+1)V_q, \tag{B.12}$$

with coefficients of (B.10) being

$$b_j = k-j+1, \quad c_q = p-q+1, \quad (k,j,p,q = 1,\ldots,N). \tag{B.13}$$

We also note the following identities for (B.13):

$$\sum_{j=1}^{k} b_j \equiv \frac{k(k+1)}{2}, \quad \sum_{j=1}^{k} b_j^2 \equiv \frac{k(k+1)(2k+1)}{6}, \\ \sum_{j=1}^{k} b_j c_j \equiv \frac{k(k+1)(2k+1)}{6} + \frac{k(k+1)(p-k)}{2}. \tag{B.14}$$

Hence, from (B.11), (B.12) and (B.14), using $\varepsilon^{-1} \equiv N+1$, we get the mean, variance and covariance of R_k:

$$\mathbb{E}[R_k] \equiv \varepsilon^{-1}\mathbb{E}[L_k] = \frac{k(k+1)}{2}, \tag{B.15a}$$

$$\mathbb{V}\mathrm{ar}[R_k] \equiv \varepsilon^{-2}\mathbb{V}\mathrm{ar}[L_k] = \frac{k(k+1)(2k+1)(N+1)}{6(N+2)} - \frac{(\mathbb{E}[R_k])^2}{N+2}, \tag{B.15b}$$

$$\mathbb{C}\mathrm{ov}(R_k, R_p) \equiv \varepsilon^{-2}\mathbb{C}\mathrm{ov}(L_k, T_p) = \frac{k(k+1)(2k+1)(N+1)}{6(N+2)} + \frac{k(k+1)(p-k)(N+1)}{2(N+2)} - \\ - \frac{\mathbb{E}[R_k]\,\mathbb{E}[R_p]}{N+2}, \quad k \leqslant p. \tag{B.15c}$$

Acknowledgements

The authors would like to gratefully acknowledge the financial support of the AirPROM 7th European Framework and the Marie Curie Network MMBNOTT (Project No. MEST-CT-2005-020723) (ILC) and the Leverhulme Trust (OEJ).

References

ACRIVOS, A., HINCH, E. J. & JEFFREY, D. J. (1980) Heat transfer to a slowly moving fluid from a dilute fixed bed of heated spheres. *J. Fluid Mech.*, **101**, 403–421.

ALLAIRE, G. & RAPHAEL, A.-L. (2007) Homogenization of a convection-diffusion model with reaction in a porous medium. *Comptes Rendus Mathematique*, **344**, 523–528.

AURIAULT, J.-L. & ADLER, P. M. (1995) Taylor dispersion in porous media: Analysis by multiple scale expansions. *Adv. Water Resour.*, **18**, 217–226.

BABUŠKA, I. (1976) Solution of interface problems by homogenization. I. *SIAM J. Math. Anal.*, **7**, 603–634.

BAKHVALOV, N. S. (1974) Averaged characteristics of bodies with periodic structure. *Soviet Physics Doklady*, **19**, 650.

BAKHVALOV, N. S. & PANASENKO, G. P. (1989) *Homogenisation: Averaging Processes in Periodic Media; Mathematical Problems in the Mechanics of Composite Materials, Mathematics and its applications*, vol. 36. Dordrecht: Kluwer Academic Publishers, 366 pp.

BAL, G. & JING, W. (2010) Homogenization and corrector theory for linear transport in random media. *Discret. Contin. Dyn. Syst.*, **28**, 1311–1343.

BATCHELOR, G. K. & O'BRIEN, R. W. (1977) Thermal or electrical conduction through a granular material. *Proc. R. Soc. Lond. A*, **355**, 313–333.

BENSOUSSAN, A., LIONS, J.-L. & PAPANICOLAOU, G. (1978) *Asymptotic Analysis for Periodic Structures, Studies in mathematics and its applications*, vol. 5. Elsevier North-Holland, 700 pp.

BERDICHEVSKII, V. L. (1975) Spatial averaging of periodic structures. *Soviet Physics Doklady*, **20**, 334.

BERGMAN, D. J. (1980) Exactly solvable microscopic geometries and rigorous bounds for the complex dielectric constant of a two-component composite material. *Phys. Rev. Lett.*, **44**, 1285–1287.

BOURGEAT, A. & PIATNITSKI, A. (1999) Estimates in probability of the residual between the random and the homogenized solutions of one-dimensional second-order operator. *Asymptotic Analysis*, **21**, 303–315.

CAPASSO, V. (2009) Multiple scales and geometric structures: additional sources of randomness. *J. Math. Biol.*, **59**, 143–146.

CHAPMAN, S. J., SHIPLEY, R. J. & JAWAD, R. (2008) Multiscale modeling of fluid transport in tumors. *Bull. Math. Biol.*, **70**, 2334–2357.

CHERNYAVSKY, I. L. (2011) *A Multiscale Analysis of Flow and Transport in the Human Placenta*. PhD Thesis, The University of Nottingham.

CHERNYAVSKY, I. L., LEACH, L., DRYDEN, I. L. & JENSEN, O. E. (2011) Transport in the placenta: homogenizing haemodynamics in a disordered medium. *Phil. Trans. R. Soc. A*, **369**, 4162–4182.

HASHIN, Z. & SHTRIKMAN, S. (1962) A variational approach to the theory of the effective magnetic permeability of multiphase materials. *J. Appl. Phys.*, **33**, 3125–3131.

KELLER, J. B. (1963) Conductivity of a medium containing a dense array of perfectly conducting spheres or cylinders or nonconducting cylinders. *J. Appl. Phys.*, **34**, 991–993.

KELLER, J. B. (1977) Effective behavior of heterogeneous media. E. W. Montroll & U. Landman, eds., *Statistical Mechanics and Statistical Methods in Theory and Application*, New York: Plenum Press, pp. 631–644.

KORN, G. A. & KORN, T. M. (2000) *Mathematical Handbook for Scientists and Engineers: Definitions, Theorems, and Formulas for Reference and Review*. Mineola, N.Y: Dover Publications, 1152 pp.

MADDOCKS, J. H. (2004) Bifucation theory, symmetry breaking and homogenization in continuum mechanics descriptions of DNA. D. Givoli, M. J. Grote & P. G. C., eds., *A celebration of mathematical modeling: the Joseph B. Keller anniversary volume*, Dordrecht: Kluwer, pp. 113–136.

MATSUNAWA, T. (1985) The exact and approximate distributions of linear combinations of selected order statistics from a uniform distribution. *Ann. Inst. Stat. Math.*, **37**, 1–16.

MAURI, R. (1991) Dispersion, convection, and reaction in porous media. *Phys. Fluids A*, **3**, 743–756.

MAXWELL, J. C. (1873) *A Treatise on Electricity and Magnetism*, vol. 1. Oxford: Clarendon press, 365 pp.

MCCARTY, P. & HORSTHEMKE, W. (1988) Effective diffusion coefficient for steady two-dimensional convective flow. *Phys. Rev. A*, **37**, 2112– 2117.

MCLAUGHLIN, D. W., PAPANICOLAOU, G. C. & PIRONNEAU, O. R. (1985) Convection of microstructure and related problems. *SIAM J. Appl. Math.*, **45**, 780–797.

MIKELIĆ, A., DEVIGNE, V. & VAN DUIJN, C. J. (2006) Rigorous upscaling of the reactive flow through a pore, under dominant Péclet and Damköhler numbers. *SIAM J. Math. Anal.*, **38**, 1262–1287.

MILTON, G. W. (1981) Bounds on the electromagnetic, elastic, and other properties of two-component composites. *Phys. Rev. Lett.*, **46**, 542–545.

PAPANICOLAOU, G. C. (1975) Asymptotic analysis of transport processes. *Bull. Amer. Math. Soc*, **81**, 330–392.

PARNELL, W. J. & ABRAHAMS, I. D. (2008) A new integral equation approach to elastodynamic homogenization. *Proc. R. Soc. A*, **464**, 1461–1482.

PARNELL, W. J. & ABRAHAMS, I. D. (2012) *An Introduction to Homogenization in Continuum Mechanics*. Cambridge University Press, (in press).

PAVLIOTIS, G. A. & STUART, A. M. (2008) *Multiscale Methods: Averaging and Homogenization*, *Texts in Applied Mathematics*, vol. 53. Springer, 310 pp.

PRAGER, S. (1963) Interphase transfer in stationary two-phase media. *Chem. Eng. Sci.*, **18**, 227–231.

RAYLEIGH, L. (1892) On the influence of obstacles arranged in rectangular order upon the properties of a medium. *Philosophical Magazine*, **34**, 481–502.

SÁNCHEZ-PALENCIA, E. (1980) *Non-Homogeneous Media and Vibration Theory*, *Lectures Notes in Physics*, vol. 127. Berlin: Springer-Verlag, 398 pp.

SANGANI, A. S. & ACRIVOS, A. (1982) Slow flow past periodic arrays of cylinders with application to heat transfer. *Int. J. Multiph. Flow*, **8**, 193–206.

SANGANI, A. S. & ACRIVOS, A. (1983) The effective conductivity of a periodic array of spheres. *Proc. R. Soc. Lond. A*, **386**, 263–275.

SHAPIRO, M. & BRENNER, H. (1988) Dispersion of a chemically reactive solute in a spatially periodic model of a porous medium. *Chem. Eng. Sci.*, **43**, 551–571.

SHIPLEY, R. J. & CHAPMAN, S. J. (2010) Multiscale modelling of fluid and drug transport in vascular tumours. *Bull. Math. Biol.*, **72**, 1464–1491.

TORQUATO, S. (1991) Random heterogeneous media: Microstructure and improved bounds on effective properties. *Appl. Mech. Rev.*, **44**, 37–76.

TORQUATO, S. (2006) *Random Heterogeneous Materials: Microstructure and Macroscopic Properties, Interdisciplinary Applied Mathematics*, vol. 16. New York: Springer, 701 pp., corr. 2nd printing.

WANG, W. & SANGANI, A. S. (1997) Nusselt number for flow perpendicular to arrays of cylinders in the limit of small Reynolds and large Péclet numbers. *Phys. Fluids*, **9**, 1529–1539.

WHITAKER, S. (1967) Diffusion and dispersion in porous media. *AIChE Journal*, **13**, 420–427.

WOOD, B. D., QUINTARD, M. & WHITAKER, S. (2002) Calculation of effective diffusivities for biofilms and tissues. *Biotechnol. Bioeng.*, **77**, 495–516.

ZHIKOV, V. V., KOZLOV, S. M., OLEINIK, O. A. & NGOAN, K. T. (1979) Averaging and G-convergence of differential operators. *Rus. Math. Surv.*, **34**, 69–147.

ZOLOTAREV, P. P. & RADUSHKEVICH, L. V. (1968) The equations for dynamic sorption in an undeformed porous medium. *Doklady Phys. Chem.*, **182**, 643–646.